The Plant Cell, Vol. 31: 3015–3032, December 2019, www.plantcell.org © 2019 ASPB.

Secretion of Phospholipase Dδ Functions as a Regulatory Mechanism in Plant Innate Immunity[OPEN]

Jingjing Xing,[a,b,1] Xiaojuan Li,[a,c,1] Xiaohua Wang,[a] Xueqin Lv,[c] Li Wang,[a] Liang Zhang,[a] Yingfang Zhu,[b] Qianhua Shen,[d] František Baluška,[e] Jozef Šamaj,[f] and Jinxing Lin[a,c,2]

[a] Institute of Botany, Chinese Academy of Sciences, Beijing 100093, China
[b] Key Laboratory of Plant Stress Biology, School of Life Sciences, Henan University, Kaifeng 457004, China
[c] Beijing Advanced Innovation Center for Tree Breeding by Molecular Design and College of Biological Sciences and Biotechnology, Beijing Forestry University, Beijing 100083, China
[d] State Key Laboratory of Plant Cell and Chromosome Engineering, Centre for Molecular Agrobiology, Institute of Genetics and Developmental Biology, Chinese Academy of Sciences, Beijing100101, China
[e] Institute of Cellular and Molecular Botany, Rheinische Friedrich-Wilhelms-University Bonn, Department of Plant Cell Biology, Bonn D-53115, Germany
[f] Centre of the Region Hana for Biotechnological and Agricultural Research, Faculty of Science, Palacky University, Olomouc 78301, Czech Republic

ORCID IDs: 0000-0002-9436-0423 (J.J.X.); 0000-0002-9955-2467 (X.J.L.); 0000-0003-2320-4543 (X.H.W.); 0000-0003-3432-2166 (X.Q.L.); 0000-0003-1688-064X (L.W.); 0000-0003-1611-3205 (L.Z.); 0000-0003-4313-1708 (Y.F.Z.); 0000-0002-9446-3086 (Q.-H.S.); 0000-0001-8763-7861 (F.B.); 0000-0003-4750-2123 (J.S.); 0000-0001-9338-1356 (J.X.L.)

Plant phospholipase Ds (PLDs), essential regulators of phospholipid signaling, function in multiple signal transduction cascades; however, the mechanisms regulating PLDs in response to pathogens remain unclear. Here, we found that Arabidopsis (*Arabidopsis thaliana*) PLDδ accumulated in cells at the entry sites of the barley powdery mildew fungus, *Blumeria graminis* f. sp *hordei*. Using fluorescence recovery after photobleaching and single-molecule analysis, we observed higher PLDδ density in the plasma membrane after chitin treatment; PLDδ also underwent rapid exocytosis. Fluorescence resonance energy transfer with fluorescence lifetime imaging microscopy showed that the interaction between PLDδ and the microdomain marker AtREMORIN1.3 (AtREM1.3) increased in response to chitin, indicating that exocytosis facilitates rapid, efficient sorting of PLDδ into microdomains upon pathogen stimulus. We further unveiled a trade-off between brefeldin A (BFA)–resistant and –sensitive pathways in secretion of PLDδ under diverse conditions. Upon pathogen attack, PLDδ secretion involved syntaxin-associated VAMP721/722-mediated exocytosis sensitive to BFA. Analysis of phosphatidic acid (PA), hydrogen peroxide, and jasmonic acid (JA) levels and expression of related genes indicated that the relocalization of PLDδ is crucial for its activation to produce PA and initiate reactive oxygen species and JA signaling pathways. Together, our findings revealed that the translocation of PLDδ to papillae is modulated by exocytosis, thus triggering PA-mediated signaling in plant innate immunity.

INTRODUCTION

Phospholipids, the bilayer-forming structural components of membranes, have novel and unexpected roles in cell signaling (Wang and Chapman, 2013). The phospholipase D (PLD) family of enzymes, which directly generate phosphatidic acid (PA) through the hydrolysis of structural phospholipids, plays a vital role in lipid-based signaling cascades in plants. Arabidopsis (*Arabidopsis thaliana*) has 12 genes that encode PLDs of six types (three genes for PLDα, two for PLDβ, three for PLDγ, one for PLDδ and PLDε, and two for PLDζ), and these types have distinguishable biochemical and regulatory properties (Zhang et al., 2003; Hong et al., 2016; Takáč et al., 2019). Considerable work has focused on the regulatory functions of PLD signaling pathways, which alter cellular and physiological processes in response to different stimuli, including abscisic acid, auxin, reactive oxygen species, and freezing (Zhang et al., 2003; Li et al., 2004; Bargmann and Munnik, 2006; Mishra et al., 2006; Guo et al., 2012). Distinct from other PLDs, PLDδ is activated by oleic acid and serves as a direct link between the plasma membrane (PM) and the microtubule cytoskeleton (Gardiner et al., 2001; Wang and Wang, 2001; Pleskot et al., 2013). Previous studies of the specific properties of PLDδ have focused on its role in the responses to abiotic stresses, such as tolerance of freezing, dehydration, and high-salt stress, as well as in abscisic acid–induced leaf senescence (Katagiri et al., 2001; Li et al., 2004; Jia et al., 2013).

Increasing evidence suggests that phospholipid-derived molecules and PLD enzymes play roles in plant–pathogen interactions (Laxalt and Munnik, 2002; Kachroo and Kachroo, 2009; Pinosa et al., 2013). For example, in rice (*Oryza sativa*) challenged with the bacterial pathogen *Xanthomonas oryzae*, PLDα1-like PLDs cluster in the PM adjacent to the bacterial cells in leaves

[1] These authors contributed equally to this work.
[2] Address correspondence to linjx@ibcas.ac.cn.
The author responsible for distribution of materials integral to the findings presented in this article in accordance with the policy described in the Instructions for Authors (www.plantcell.org) is: Jinxing Lin (linjx@ibcas.ac.cn).
[OPEN]Articles can be viewed without a subscription.
www.plantcell.org/cgi/doi/10.1105/tpc.19.00534

IN A NUTSHELL

Background: Penetration resistance, a key aspect of plant innate immunity, hinders fungi from entering the plant and involves a well-described innate immunity process that depends on the formation of papillae. As a member of the phospholipase D (PLD) family of enzymes in plants, PLDδ acts as the main isoform in the penetration resistance of Arabidopsis to barley powdery mildew fungi (*Blumeria graminis* f. sp. *hordei*, *Bgh*), with a striking accumulation at the attempted *Bgh* penetration sites. As the pivotal regulator of phospholipid signaling, the distinct location of PLD is closely associated with its function; nevertheless, the regulatory mechanisms and the relocalization of PLDδ in response to pathogens remain poorly understood.

Question: Numerous studies have focused on the role of phosphatidic acid in activating downstream signaling in plant defense, but the subcellular trafficking and regulatory details of PLDδ in response to pathogens have yet to be fully elucidated.

Findings: Here, we show that *Arabidopsis thaliana* PLDδ accumulated at the entry sites of *Bgh*. Single-particle analysis revealed a higher density of PLDδ in the plasma membrane after chitin treatment, and PLDδ underwent rapid and massive exocytosis. Fluorescence resonance energy transfer with fluorescence lifetime imaging microscopy (FRET-FLIM) showed that exocytosis facilitated the nanoscale aggregation of pathogen-triggered PLDδ within AtREM1.3-labeled microdomains. The secretion of PLDδ occurred by both Brefeldin A (BFA)-resistant and sensitive pathways and BFA-sensitive secretion increased significantly in response to pathogen. Upon pathogen attack, PLDδ was secreted via SNARE-mediated exocytosis sensitive to BFA. By analyzing phosphatidic acid, H_2O_2 and jasmonic acid (JA) levels, and expression of related genes, we further unveiled that the translocation of PLDδ is crucial to trigger reactive oxygen species and JA signaling pathways. Together, our findings illustrate a novel regulatory mechanism involving exocytosis in the transport of PLDδ, aiding in the execution of penetration resistance against a fungal pathogen.

Next steps: Previous studies reported that the local production of PA by PLDs induces negative curvature of the membrane and recruits other proteins for membrane fusion. In our further studies, we will focus on the function of PLDδ-PA in membrane fusion of plant exosomes in papillae. We will also investigate whether SNARE-mediated exocytosis is influenced by accumulation of PLDδ-PA at the pathogen entry sites.

undergoing an immune response. The translocation of PLDs in response to pathogen attack suggests that these PLDs are activated in response to pathogens and function in the resistance interaction (Young et al., 1996; Wang et al., 2006). PA, a vital signaling lipid produced by PLD, has also been reported to activate multiple cellular responses in plant defense, including the oxidative burst and mitogen-activated protein kinase cascades (Rizzo et al., 2000; Rentel et al., 2004). Furthermore, PA accumulates in response to pathogen-associated molecular patterns (PAMPs), inducing pathogen-related gene expression and cell death (Testerink and Munnik, 2011). As PLD is a pivotal regulator of phospholipid signaling in plant cells, its location is closely associated with its function.

Plant innate immunity endows entire species of plants with resistance to potentially infectious pathogens, such as viruses, bacteria, and fungi. Epidermal penetration resistance, a key aspect of innate immunity, hinders fungi from entering the plant and involves the localized formation of cell wall appositions known as papillae (Nielsen et al., 2012). In Arabidopsis, two separate pathways enhance penetration resistance: one pathway involves syntaxin (PEN1) and the other involves a combination of peroxisomal β-glycosyl hydrolase (PEN2) and the PM-localized ATP-binding cassette transporter PEN3 (Lipka et al., 2005, 2008; Stein et al., 2006; Clay et al., 2009). During these well-described plant defense processes, PLDδ is also reported to be involved in the basal defense and nonhost resistance response (Pinosa et al., 2013). Nevertheless, the functions of phospholipid signaling pathways during these plant defense processes have remained largely unknown, and the translocation of PLDδ and downstream signaling in the Arabidopsis–*Blumeria graminis* f. sp *hordei* (*Bgh*) plant–fungus interactions remain to be further elucidated.

Previous studies have focused on the functions of PA in plant defense signaling (Rizzo et al., 2000; Rentel et al., 2004); however, the relocalization and accumulation of PLDδ in response to pathogens remained to be examined and may be a key step for signal transmission in plant innate immunity. In this study, we examined PLDδ exocytosis in plant innate immunity during plant–pathogen interactions, with particular emphasis on the spatio-temporal dynamics of PLDδ translocation. Furthermore, we explored whether the partitioning of PLDδ in plant defense is associated with membrane microdomains. Our comprehensive analyses offer insight into the diverse regulation of PLDδ secretion in penetration resistance and may also serve as a model of how membrane phospholipases control phospholipid signaling in response to pathogens.

RESULTS

PLDδ Aggregates in PM Microdomains during *Bgh* Infection

To characterize the subcellular localization of Arabidopsis PLDδ in penetration resistance against *Bgh*, we expressed a PLDδ-green fluorescent protein (GFP) fusion under the control of the 35S promoter and the native *PLDδ* promoter in the wild type and *pldδ* mutants. To test whether PLDδ-GFP retained function, we then examined the resistance phenotype of the wild-type Columbia (Col-0), *p35S:PLDδ-GFP*/Col-0, *pPLDδ:PLDδ-GFP*/*pldδ*, and *pldδ* plants. Measurement of penetration rates and

hypersensitive response–associated cell death in *Bgh*-infected leaves showed that PLDδ-GFP retained function and PLDδ was required for penetration resistance (Supplemental Figure 1). We further analyzed the subcellular localization of PLDδ-GFP using confocal laser scanning microscopy. Upon *Bgh* infection, a striking accumulation of PLDδ-GFP was observed at the *Bgh* penetration sites and GFP signal remained localized at the papillae in the extracellular space after plasmolysis (Figures 1A to 1G). When the membrane in the papillae was stained with the fluorescent lipophilic dye FM4-64, the red signal of this dye overlapped with the GFP signal at penetration sites, revealing colocalization of the preformed papillae with PLDδ-GFP (Figures 1H to 1K). These results showed that PLDδ was targeted mainly to the membranes of papillae in the extracellular space during infection by *Bgh.*

To study the role of PLDδ in defense responses, we treated the plants with the fungal elicitor chitin, as described previously (Underwood and Somerville, 2013), and used fluorescence correlation spectroscopy (FCS) to measure the density of PLDδ-GFP in the PM in vivo (Li et al., 2011). We found that the average density of PLDδ-GFP in the PM was 7.9 ± 0.5 molecules μm^{-2} in the resting condition (no chitin) but that of the chitin-treated cells was 44% higher, at 14.1 ± 1.5 molecules μm^{-2}. Cycloheximide (CHX), an inhibitor of de novo protein synthesis, suppressed this increase, resulting in a PLDδ-GFP protein density of only 5.7 ± 0.1 molecules μm^{-2} in plants treated with CHX plus chitin (Figures 2A and 2B). Moreover, immunoblot analysis showed that the abundance of PLDδ-GFP increased in response to chitin in the PM and in the entire cell and that CHX pretreatment inhibited this rise (Figure 2C; Supplemental Figure 2). Using total internal reflection fluorescence microscopy (TIRFM), we found that the fluorescence intensities of PLDδ-GFP at the PM were not homogeneous and more PLDδ-GFP aggregation foci occurred in the chitin-treated plants (Figures 2D and 2E).

To determine how the cell recruited PLDδ-GFP to the PM, we examined the dynamics of PLDδ-GFP within the PM using fluorescence recovery after photobleaching (FRAP). The FRAP analysis showed that in the chitin-treated cells, PLDδ-GFP had a shorter average half-life ($t_{1/2,\ chitin}$ = 5.93 ± 0.29 min; $t_{1/2,\ control}$ = 7.36 ± 0.35 min) in the PM and a higher percentage of recovery (chitin treated, 38.82 ± 1.51%; control, 33.64 ± 0.97%) compared with the resting condition (Figures 2F and 2G). The fluorescence recovery curve of membrane-resident proteins describes the sum of the lateral mobility of the protein in the membrane and the exchange of proteins between cytoplasmic vesicles and the membrane via exocytosis and endocytosis.

To separate these effects, we divided the initial bleaching regions into top, middle, and bottom sectors; lateral mobility from adjacent membrane regions will preferentially increase recovery in the top and bottom sectors, but exocytosis-mediated exchange will contribute evenly to all three sectors. We found that the three regions recovered at equal rates (Supplemental Figures 3A to 3D; Supplemental Table). When we photobleached GFP signals on the cell surface and measured FRAP signals from the center, the periphery, and the entirety of the bleached areas over time, the results showed that these three regions also recovered at equal rates (Supplemental Figure 4). These results indicated that PLDδ-GFP is primarily recruited from the cytoplasm to the PM via exocytosis; therefore, the rate of recovery represents the rate of exocytosis. Moreover, we examined the regions next to the bleached regions (magenta circles in Supplemental Figure 4) and found that the fluorescence signal was increased by chitin treatments compared with that under control conditions (Supplemental Figure 4). Based on this, we found that the exocytosis rate of PLDδ-GFP showed a 15% increase in chitin-treated cells compared with the control cells (Figure 2H).

Protein Sorting into Microdomains Is Related to the Focal Accumulation of PLDδ

PMs are highly organized structures that contain diverse coexisting microdomains (Jarsch et al., 2014), and previous proteomics studies have detected PLDδ in the detergent-resistant membrane fraction from plants (Shahollari et al., 2005; Demir et al., 2013). To investigate whether the localization of PLDδ is associated with microdomains during penetration resistance, we used AtREMORIN1.3 (AtREM1.3) as a marker of sterol-rich membrane microdomains and created transgenic plants coexpressing AtREM1.3-mCherry and PLDδ-GFP. At 48 hours postinfection (hpi) with *Bgh*, AtREM1.3-mCherry accumulated in the papillae and colocalized with the accumulation of PLDδ-GFP in foci (Figures 3A to 3D), implying that the papillary extracellular membrane also included microdomains and that PLDδ was contained within these microdomains during the penetration resistance response.

We quantified the colocalization of AtREM1.3-mCherry and PLDδ-GFP using the protein proximity index (PPI), revealing that the mean PPI value for PLDδ-GFP and AtREM1.3-mCherry was 0.90 ± 0.05 after chitin exposure but only 0.66 ± 0.06 in the resting condition. This indicated that the degree of colocalization between PLDδ-GFP and AtREM1.3-mCherry increased from more than moderate to very strong during the PAMP response (Figures 3E to 3I).

We further used fluorescence resonance energy transfer with fluorescence lifetime imaging microscopy (FRET-FLIM) to confirm the interaction between PLDδ-GFP and AtREM1.3-mCherry. The fluorescence lifetime of PLDδ-GFP alone in the PM of epidermal cells was ~2.38 ± 0.04 ns. In the transgenic line coexpressing free-GFP and AtREM1.3-mCherry, the mean GFP fluorescence lifetime of free-GFP (2.35 ± 0.05 ns) showed no meaningful difference from that of PLDδ-GFP alone. However, the average GFP fluorescence lifetime was strongly reduced in the plants coexpressing PLDδ-GFP and AtREM1.3-mCherry (2.23 ± 0.04 ns). After treatment with chitin, the fluorescence lifetime of PLDδ-GFP in these plants showed a strong reduction (to 1.98 ± 0.06 ns) in comparison to the coexpressing plants in the control condition, with a FRET efficiency of 16.7% (Figures 3J to 3N).

To better understand the molecular mechanisms underlying the partitioning of PLDδ into PM microdomains, we investigated the dynamic behavior of individual PLDδ-GFP fluorescent spots inside living cells using single-particle tracking in continuous images (Supplemental Figures 5A and 5C; Supplemental Movies S1 and S2). Next, we obtained histograms of the diffusion coefficients, which we measured by fitting the particle trajectories to

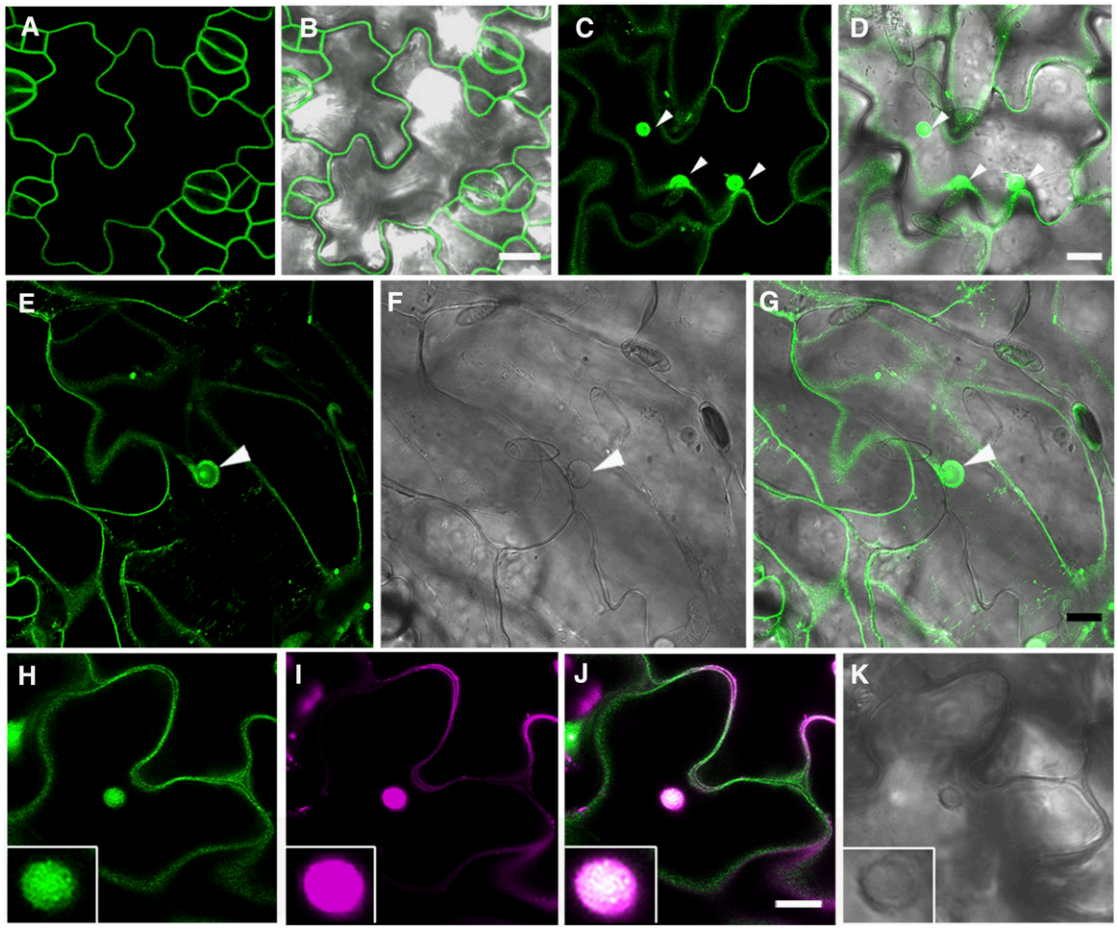

Figure 1. Subcellular Localization of PLDδ-GFP following *Bgh* Infection.

(A) and **(B)** Fluorescence **(A)** and fluorescence merged with bright-field **(B)** images showing that PLDδ-GFP is localized at the epidermal cell membrane of the control Arabidopsis leaves.

(C) and **(D)** Fluorescence **(C)** and fluorescence merged with bright-field **(D)** images demonstrating the localization of PLDδ-GFP at the *Bgh* penetration sites. The white arrowheads indicate the accumulation of PLDδ-GFP.

(E) to **(G)** Plasmolysis upon *Bgh* infection showed the focal accumulation (arrowhead) of PLDδ-GFP in the papillae of the periplasmic space. The fluorescence image **(E)** is merged with the bright-field image **(F)** in **(G)**.

(H) to **(K)** Focal accumulation of PLDδ-GFP **(H)** overlaps completely **(J)** with the FM4-64–stained papillae **(I)** at 48 hpi with *Bgh*. **(K)** Bright-field image of the papillae in **(H)** to **(J)**. Bar in **(B)**, **(D)**, **(G)**, and **(J)** = 10 μm.

a Gaussian function to characterize the global mobility of fluorescent spots in each treatment group, in which the Gaussian peaks ($\hat{G}$) were defined as the characteristic values for the diffusion coefficients (Cui et al., 2018; Wu et al., 2019). Under control conditions (no chitin), the diffusion coefficients of PLDδ-GFP reflected two populations, with $\hat{G}$ values of 9.55×10^{-3} μm²/s (47.13%, SE = 8.51×10^{-3} to 1.07×10^{-2} μm²/s) and 4.67×10^{-3} μm²/s (52.86%, SE = 3.98 to 5.50×10^{-3} μm²/s; Supplemental Figure 5E). Under chitin treatment, the pattern was the same, with $\hat{G}$ values of 9.77×10^{-3} μm²/s (58.69%, SE = 9.33×10^{-3} to 1.02×10^{-2} μm²/s) and 4.57×10^{-3} μm²/s (41.30%, SE = 4.27 to 4.90×10^{-3} μm²/s; Supplemental Figure 5E).

By contrast, in seedlings treated with methyl-β-cyclodextrin (MβCD), a sterol-disrupting reagent, TIRFM analysis of the PLDδ-GFP fluorescent spots revealed that the histogram of diffusion coefficients yielded a one-population distribution, with a $\hat{G}$ value of 8.91×10^{-3} μm²/s (SE = 8.79 to 9.03×10^{-3} μm²/s) in MβCD-treated cells and a $\hat{G}$ value of 9.12×10^{-3} μm²/s (SE = 8.95 to 9.29×10^{-3} μm²/s) in cells pretreated with MβCD and then treated with chitin (Supplemental Figure 5E; Supplemental Movies S3 and S4). Thus, MβCD treatment caused the percentage of PLDδ-GFP fluorescent spots with a fast diffusion coefficient to increase and caused the subpopulation with the slow diffusion coefficient to disappear.

Evaluating the diffusion mode by analyzing the mean square displacement (MSD) of the trajectories of individual PLDδ-GFP molecules over time (Supplemental Figure 5G), we found that most PLDδ-GFP molecules were restricted to specific zones and had restricted diffusion with or without chitin treatment. After pretreatment with MβCD, the movement type of PLDδ-GFP

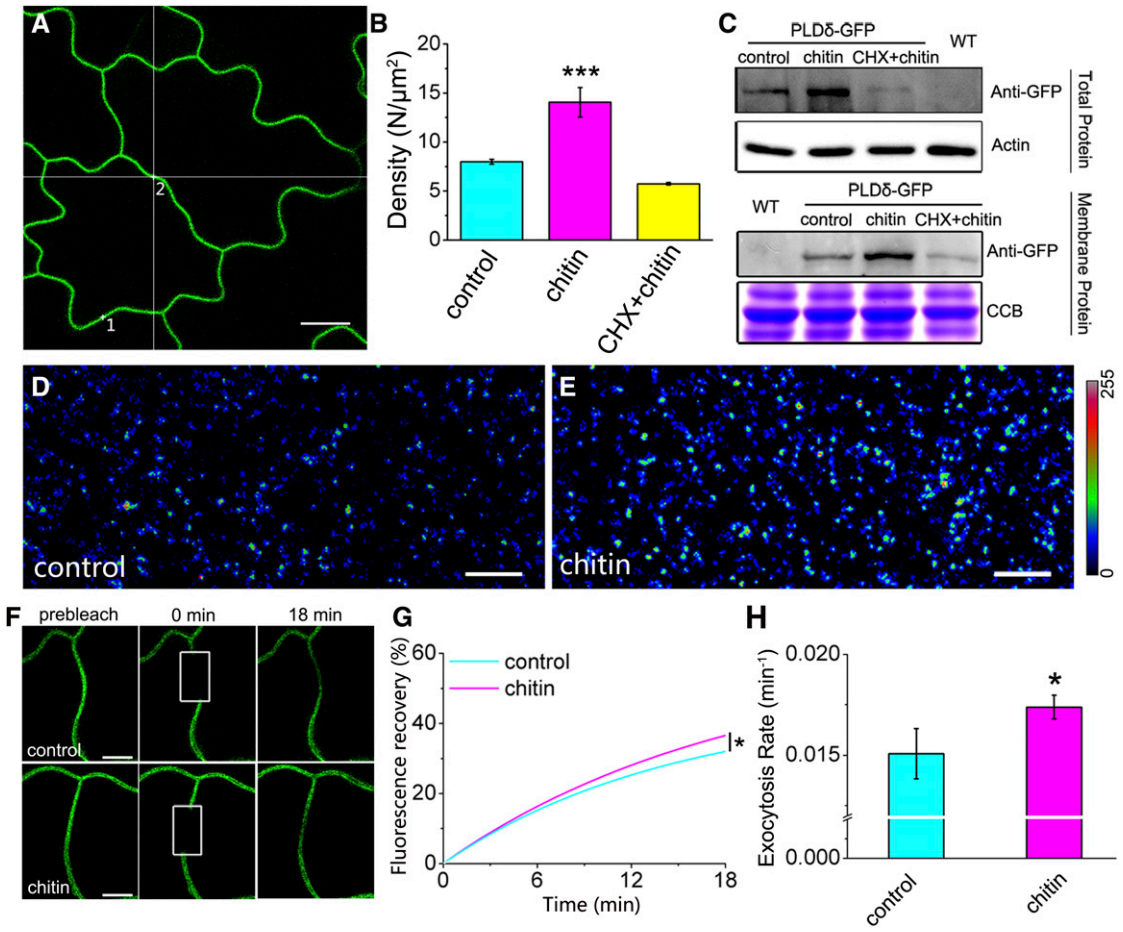

Figure 2. Density and Dynamics of PLDδ-GFP at the PM.

(A) Live-cell imaging of leaf epidermal cells expressing PLDδ-GFP, with the numbers indicating the detection areas for FCS analysis.

(B) FCS analysis determined the differences in PLDδ-GFP density at the PM following treatment with chitin or CHX plus chitin (n = 50, 96, and 74 measurements for the control, chitin, and CHX plus chitin, respectively, from 12 seedlings for each condition). ***$P < 0.001$, ANOVA and post hoc Tukey's test.

(C) Immunoblot analysis showed the abundance of PLDδ-GFP in total proteins and membrane proteins in response to chitin or CHX plus chitin treatment. Actin and Coomassie Brilliant Blue were used as the internal controls. CBB, Coomassie Brilliant Blue; WT, wild type.

(D) and **(E)** Distribution of PLDδ-GFP particle fluorescence on the PM in the control **(D)** or chitin-treated cells **(E)** shown by pseudocolor images (blue-yellow-red palette).

(F) FRAP time course of PLDδ-GFP with or without chitin treatment. White squares indicate bleached regions.

(G) Fluorescence recovery curves of the photobleached region of interest.

(H) Exocytosis rates of PLDδ-GFP with or without chitin treatment. *$P < 0.05$, Student's t test. Bars represent means, error bars represent SE. Bar = 10 μm in **(A)** and **(F)**; bar = 3 μm in **(D)** and **(E)**.

molecules changed from restricted diffusion to Brownian diffusion (Supplemental Figure 5G). Moreover, we performed experiments to examine whether the PLDδ-generated PA was affected by the sterol-enriched microdomain location. When the membrane sterol was predepleted by MβCD treatment, PLD activity was decreased and the chitin-induced PA production was reduced compared with the chitin treatment without MβCD (Supplemental Figure 6).

To test the effect of membrane microdomain disruption on the recruitment of PLDδ-GFP to sites of attempted penetration by *Bgh*, we syringe infiltrated leaves with different concentrations of MβCD 1 h before inoculation with *Bgh* and then observed the localization of PLDδ-GFP at *Bgh* penetration sites at 48 hpi (Supplemental Figures 7A and 7B). Increasing MβCD concentrations caused progressively lower PLDδ-GFP accumulation rates, ranging from 39.8 ± 0.6% for leaves treated with 0.5 μM MβCD to 16.8 ± 1.9% at 2 μM MβCD (Supplemental Figure 7C). We also determined the impact of MβCD on *Bgh* penetration and found that MβCD treatment increased the penetration rate to 19.81 ± 1.04%, approximately twice that measured after control treatment with double-distilled water (10.07 ± 1.19%; Supplemental Figure 8A).

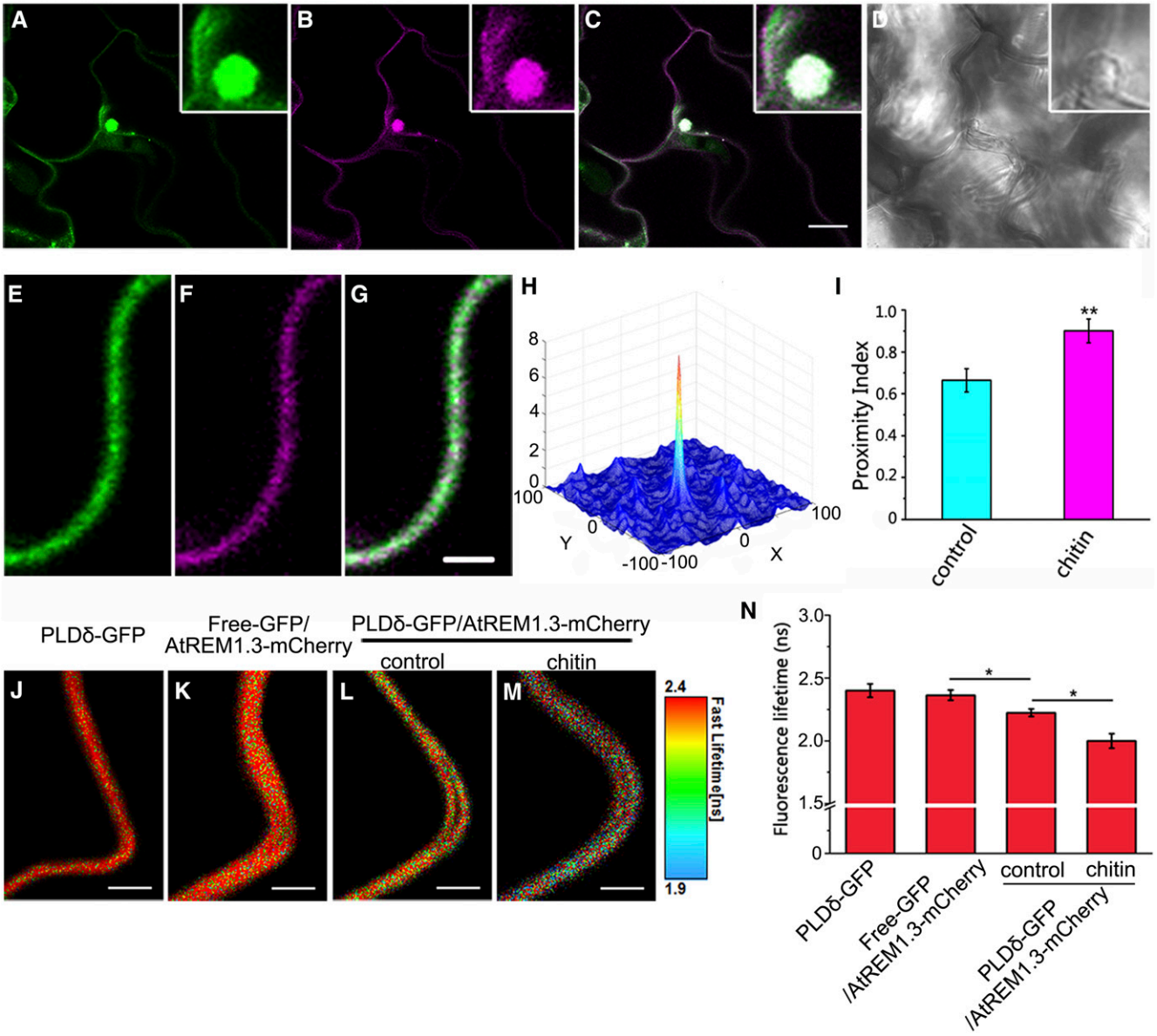

Figure 3. Localization of PLDδ-GFP in PM Microdomains.

(A) to **(D)** Colocalization of PLDδ-GFP **(A)** and AtREM1.3-mCherry **(B)** in the papillae, with merged **(C)** and bright-field **(D)** images.
(E) to **(G)** Live-cell imaging of leaf epidermal cells expressing PLDδ-GFP **(E)**, AtREM1.3-mCherry **(F)**, and the merged image **(G)** in the control conditions.
(H) and **(I)** 3D cross-correlation plot of PLDδ-GFP and AtREM1.3-mCherry as a function of pixel shift **(H)**. PPI between PLDδ-GFP and AtREM1.3-mCherry with or without chitin treatment **(I)**. ($n = 10$, with 15 regions of interest in the control condition and 30 in the chitin treatment).
(J) to **(M)** Live-cell imaging (using confocal microscopy) of fluorescence lifetime distribution of PLDδ-GFP in the plants expressing PLDδ-GFP alone **(J)**, coexpressing free-GFP/AtREM1.3-mCherry **(K)**, and coexpressing PLDδ-GFP/AtREM1.3-mCherry. **(L)** and **(M)** indicate the fluorescence lifetime of PLDδ-GFP with **(L)** or without chitin treatment **(M)**. AtREM1.3 is a marker of membrane microdomains.
(N) FRET-FLIM analysis revealed the fluorescence lifetime of PLDδ-GFP ($n = 12$, with 15 regions of interest in the plants expressing PLDδ-GFP alone and 15 regions in the plants coexpressing PLDδ-GFP/AtREM1.3-mCherry under control conditions and 19 under chitin treatment). Bars represent means; error bars in all panels represent SD. *$P < 0.05$, **$P < 0.01$, ***$P < 0.001$ (Student's *t* test in **[H]**; ANOVA and post hoc Tukey's test in **[K]**). Bar = 10 μm in **(A)** to **(G)**; bar = 2 μm in **(J)** to **(M)**.

Pathogen-Inducible PLDδ Recruited in a BFA-Sensitive Manner

Since exocytosis of PLDδ increased in response to pathogen, we next tried to identify the secretory pathway that traffics PLDδ to the papillae. We used the vesicle-trafficking inhibitor brefeldin A (BFA), which inhibits certain ADP ribosylation factor/guanine nucleotide exchange factors, to address this question. In plants treated with 50 μM BFA plus FM4-64, PLDδ-GFP showed weak intracellular agglomeration that colocalized with positive BFA compartments labeled with FM4-64. In addition, most punctate PLDδ-GFP structures were intact and did not accumulate in BFA bodies (Figures 4A to 4C). Exposure of seedlings to chitin after BFA pretreatment led to an obvious accumulation of PLDδ-GFP in BFA bodies, but many PLDδ-GFP signals remained unaffected by BFA (Figures 4D to 4F). Quantitative analysis of PLDδ exocytosis showed that the numbers of BFA bodies labeled with PLDδ-GFP increased to 481.20% of control in response to chitin exposure, but the numbers of BFA-resistant vesicles marked by PLDδ-GFP did not significantly change under either control or chitin treatment conditions (Figures 4G and 4H). Cells pretreated with CHX had fewer BFA-resistant vesicles and BFA bodies labeled by PLDδ-GFP (Supplemental Figure 9), indicating that the secretion of PLDδ involved BFA-resistant and -sensitive pathways that were both derived from de novo protein synthesis. FRAP analysis also showed that the average half-life increased from 5.93 ± 0.29 to 7.27 ± 0.26 min, and the percentage of recovery decreased from 38.82 ± 1.51 to 29.21 ± 1.73% in plants treated with chitin following BFA pretreatment (Figures 4I to 4L). In addition, we detected a 24.7% decrease of the exocytosis rate in the presence of BFA (Figure 4M).

To further investigate whether PLDδ-GFP was associated with BFA-sensitive secretion during *Bgh* attack, we syringe infiltrated leaves with 300 μM BFA 1 h before inoculation with *Bgh* and observed the localization of PLDδ-GFP at *Bgh* penetration sites at 48 hpi. In the BFA-treated leaves, PLDδ-GFP often did not accumulate at the sites of attempted *Bgh* penetration (Figures 4N and 4O), and the frequency of normal papillary PLDδ-GFP accumulation decreased from 90.3 ± 5.1 to 25.8 ± 6.2% (Figure 4P). Moreover, BFA treatment lead to an increase in the penetration rate of *Bgh* (Supplemental Figure 8B).

Bgh-Triggered PLDδ Associates with PEN1 in Vivo at the PM and Papillary Extracellular Membrane

Previous studies revealed that treatment with BFA blocks the accumulation of PEN1 (Nielsen et al., 2012); therefore, we next asked whether the trafficking pathway of PLDδ is associated with PEN1. In the transgenic plants coexpressing PLDδ-GFP and mCherry-PEN1, PLDδ and PEN1 clearly colocalized at the preformed papillae after *Bgh* inoculation (Figures 5A to 5D). PPI was used to quantify the fraction of colocalized molecules in these plants, revealing a mean value of 0.23 ± 0.05 for the proximity of PLDδ-GFP to mCherry-PEN1 in the resting condition, which increased to 0.63 ± 0.07 after treatment with chitin (Supplemental Figures 10A to 10E), representing a change in the degree of colocalization between PLDδ and PEN1 from weak to more than moderate. We also used FLIM to detect FRET between PLDδ-GFP and mCherry-PEN1 in the PM of epidermal cells. FRET-FLIM analysis revealed a reduction in the fluorescence lifetime of PLDδ-GFP from 2.39 ± 0.05 ns in the PLDδ-GFP–expressing plants to 2.22 ± 0.02 ns in the PLDδ-GFP/mCherry-PEN1–coexpressing plants, whereas the GFP fluorescence lifetime did not decrease in the transgenic lines coexpressing free-GFP/mCherry-PEN1 (2.36 ± 0.04 ns).

When the PLDδ-GFP/mCherry-PEN1–coexpressing plants were treated with chitin for 1 h, the fluorescence lifetime of PLDδ-GFP further decreased to 1.99 ± 0.05 ns and yielded a FRET efficiency of 17.0%, indicating that chitin enhanced the interaction of PLDδ and PEN1 (Figures 5E to 5I). Using coimmunoprecipitation to analyze the possible interaction between PLDδ and PEN1, we found that mCherry-PEN1 immunoprecipitated with PLDδ-GFP in transgenic plants coexpressing the two proteins, indicating that PEN1 interacts with PLDδ in vivo (Figure 5J).

PLDδ Is Trafficked to the Papillae via VAMP721/722-Mediated Secretion

PEN1 interacts with VAMP721/722 to mediate a pathway involved in secretion for the execution of penetration resistance (Kwon et al., 2008b); therefore, we hypothesized that PLDδ may share the same exocytosis pathway as PEN1 or play a role in the function of the PEN1–SNAP33–VAMP721 complex. We generated transgenic plants coexpressing PLDδ-GFP and mCherry-VAMP721 to further confirm the pathway is involved in trafficking of PLDδ. At 48 hpi with *Bgh*, PLDδ-GFP and mCherry-VAMP721 colocalized in the papillae (Figures 6A to 6D). More importantly, of the 173 PLDδ-GFP–labeled compartments observed in the cytoplasm, 153 (88.4%) colocalized with cytoplasmic bodies labeled with mCherry-VAMP721 after treatment with chitin for 1 h (Figures 6E to 6J). Similar phenomena were observed in the transgenic plants coexpressing PLDδ-GFP and mCherry-VAMP722 (Supplemental Figures 11A to 11J).

To investigate whether trafficking of PLDδ protein to the papillae is affected by VAMP721/722-mediated secretion, we obtained PLDδ-GFP *vamp721*$^{-/-}$, PLDδ-GFP *vamp722*$^{-/-}$, PLDδ-GFP *vamp721*$^{+/-}$ *vamp722*$^{-/-}$, and PLDδ-GFP *vamp721*$^{-/-}$ *vamp722*$^{+/-}$ plants. In the *vamp721*$^{-/-}$, *vamp722*$^{-/-}$, *vamp721*$^{+/-}$ *vamp722*$^{-/-}$, and *vamp721*$^{-/-}$ *vamp722*$^{+/-}$ mutant backgrounds, PLDδ protein was properly targeted to papillae after incubation with *Bgh* for 48 h (Figures 6K to 6N). To quantify the effect of VAMP721/722 in PLDδ trafficking, we counted the PLDδ-GFP foci in papillae in the PLDδ-GFP *vamp721*$^{-/-}$ and PLDδ-GFP *vamp722*$^{-/-}$ plants and found that deficiency of VAMP721/722 led to decreases in the frequency of PLDδ-GFP accumulation on papillae from 78.55 ± 4.20 to 41.26 ± 3.78% in *vamp721*$^{-/-}$ and 40.94 ± 3.05% in *vamp722*$^{-/-}$ at 48 hpi (Figure 6O). Compared with the PLDδ-GFP *vamp721*$^{+/+}$ *vamp722*$^{+/+}$ control plants, the targeting efficiency of PLDδ-GFP in PLDδ-GFP *vamp721*$^{+/-}$ *vamp722*$^{-/-}$ and PLDδ-GFP *vamp721*$^{-/-}$ *vamp722*$^{+/-}$ plants further decreased, to 12.94 ± 3.02 and 16.02 ± 6.32%, respectively, at 48 hpi (Figure 6O).

PLDδ Function in Penetration Resistance Is Diminished in the Absence of the SNARE Complex

PLD-derived PA is reported to play an essential role in basal defense and nonhost resistance (Pinosa et al., 2013). Therefore,

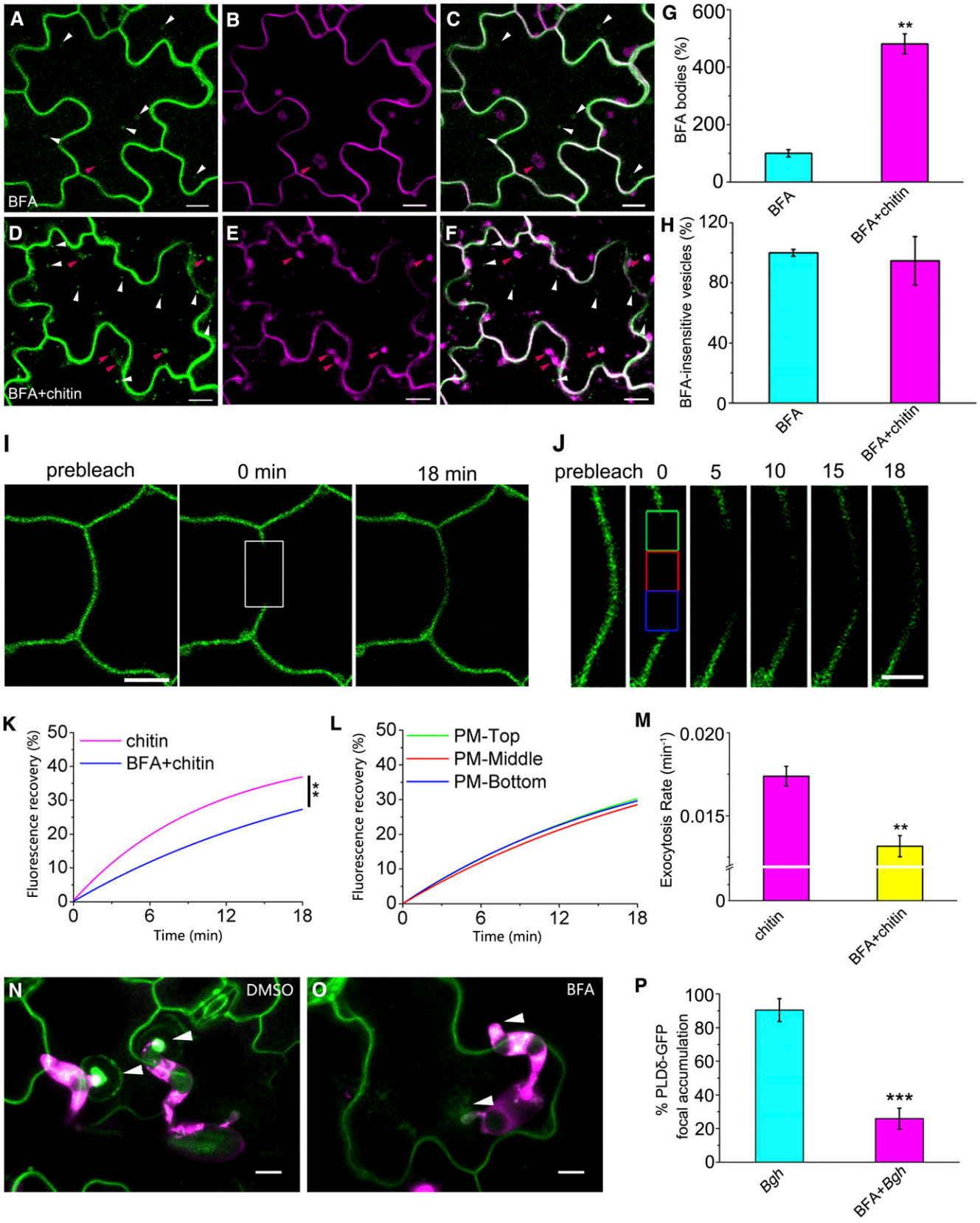

Figure 4. Effect of BFA on the Exocytosis and Accumulation of PLDδ.

we tested whether the mistargeting of PLDδ to papillae in soluble NSF-attachment protein receptors (SNARE) mutants could influence the resistance function of PLDδ. Using a biosensor based on the PA binding protein Spo20p fused to a fluorescent reporter, we found that PA accumulated in the pathogen entry site in a pattern similar to the distribution of PLDδ-GFP (Figures 7A to 7D). The *pldδ* mutants showed decreased chitin-induced PA production compared with the wild type following chitin treatment. Consistent with those observations, chitin-induced PA production was reduced in the *pen1* and *vamp721/722* mutants, as confirmed by the relative levels of phosphatidylcholine (PC) and phosphatidylethanolamine (PE), two main substrates of PLDδ, measured in *pldδ*, *pen1*, and *vamp721/722* mutants (Figure 7E; Supplemental Figure 12).

Furthermore, we analyzed the levels of hydrogen peroxide (H_2O_2) and jasmonic acid (JA) in *pldδ*, *pen1*, and *vamp721/722* mutants and the wild-type plants under chitin treatment. The *pldδ* mutants exhibited much lower H_2O_2 and JA accumulation than the wild-type plants, indicating that the loss of PLDδ disrupted the plants' ability to produce H_2O_2 and JA in response to chitin (Figure 7F; Supplemental Figure 13). More importantly, the production of H_2O_2 and JA after chitin treatment decreased in the absence of the SNARE complex (Figure 7F; Supplemental Figure 13).

To explore the molecular basis for the susceptible phenotype of *pldδ* and *snare* mutants, we tested the expression levels of the important plant defense genes *PLANT DEFENSIN GENE1.2* (*PDF1.2*), *3-PHOSPHOINOSITIDE DEPENDENT PROTEIN KINASE-1* (*PDK1.1*), *PHOSPHATE-INDUCED1.1* (*PHI1*), and *RESPIRATORY BURST OXIDASE HOMOLOG F* (*RBOHF*). RT-qPCR analysis showed that the transcript levels of *PDF1.2*, *PDK1.1*, *PTI1*, and *RBOHF* were dramatically lower in *pldδ* and *snare* mutants than in the wild-type plants (Figures 7G and 7H; Supplemental Figure 13). These results suggest that loss of function of *PEN1*, *VAMP721*, and *VAMP722* attenuates the function of PLDδ in response to pathogens.

DISCUSSION

Innate immunity helps plants defend themselves against potentially infectious pathogens, such as viruses, bacteria, and fungi. For powdery mildew fungi, resistance to penetration at the attack site of the fungus involves a well-described innate immunity process that depends on the formation of papillae, which are rich in antimicrobial compounds, at the site of attempted penetration. The strong focal accumulation of proteins involved in penetration resistance at papillae is considered to be important for their function (Assaad et al., 2004; Stein et al., 2006). In this study, we found that the loss of PLDδ caused defects in penetration resistance, in agreement with the conclusion reported recently (Zhang et al., 2018). Furthermore, we demonstrated that PLDδ was targeted to the papillary extracellular membrane, which is the extracellular site of the host membrane.

The PM provides a physical barrier for the cell and a transfer station for vesicle trafficking in many processes, including penetration resistance. Previous studies used transmission electron microscopy to reveal large numbers of exosomes, termed paramural bodies, within the papillary matrix and clusters of multivesicular bodies in close proximity to the site of pathogen attack, indicating that the trafficking destination of the multivesicular body cargos was the PM and that paramural bodies were also derived from the PM (An et al., 2006; Nielsen et al., 2012). Here, our immunoblotting assay showed a higher abundance of PLDδ-GFP protein following chitin treatment and a lower PLDδ-GFP abundance in the PM following treatment with CHX. The highly dynamic nature of PM proteins means that analyzing the density and dynamics of PLDδ molecules within living cells during the pathogen response poses a challenge; therefore, we applied single-molecule approaches with high spatial and temporal accuracy to characterize the dynamics of PLDδ in the PM. Using FCS and TIRFM analysis, we found PLDδ-GFP accumulated in the PM under pathogen stimulation. By measuring the spatial and temporal dynamics of individual fluorescent spots of PLDδ directly at the PM in living cells, our in vivo analysis offers another powerful way to understand the dynamics of PLDδ and its regulatory mechanisms.

The PM contains highly compartmentalized structures that are partitioned into different types of microdomains, which function in the transduction of various signals in plant cells, especially during the early stages of fungal infection (Bhat et al., 2005) and during other PAMP-induced signaling processes (Fujiwara et al., 2009;

Figure 4. (continued).

(A) to **(H)** Subcellular localization of PLDδ in the presence of the vesicle-trafficking inhibitor BFA with **(D)** to **(F)** or without chitin treatment (see **[A]** to **[C]**). Costaining with FM4-64 (see **[B]** and **[E]**) highlights the PM and BFA bodies. White arrowheads indicate BFA-resistant vesicles, and the magenta arrowheads indicate BFA bodies. **(G)** and **(H)** show the quantitation of BFA bodies **(G)** and BFA-resistant vesicles of PLDδ-GFP **(H)**. For each experiment, at least 30 epidermal cells from four seedlings were scored ($n = 3$).

(I) and **(J)** FRAP time course of PLDδ-GFP with BFA pretreatment and chitin treatment. The white rectangle indicates the bleached region. **(J)** The initial bleached region in **(I)** was further subdivided into three sectors, indicated by the green, red, and blue rectangles.

(K) Fluorescence recovery curves of the photobleached region of interest.

(L) Fluorescence recovery curves of divided regions of interest. Curves represent the best fits of mean values of six independent FRAP experiments on PLDδ-GFP.

(M) Exocytosis rates of PLDδ-GFP with or without BFA treatment.

(N) to **(P)** Accumulation of PLDδ-GFP at sites of *Bgh* attempted penetration with **(O)** or without pretreatment with BFA **(N)**. Arrowheads indicate the *Bgh* attempted penetration sites. For each leaf, at least 49 germinated spores were scored ($n = 3$). Bars represent means; error bars in all panels represent SD. $^{**}P < 0.01$, $^{***}P < 0.001$, Student's *t* test. Bar = 20 μm in **(A)** to **(F)**, **(N)**, and **(O)**; bar = 10 μm in **(I)**; bar = 5 μm in **(J)**.

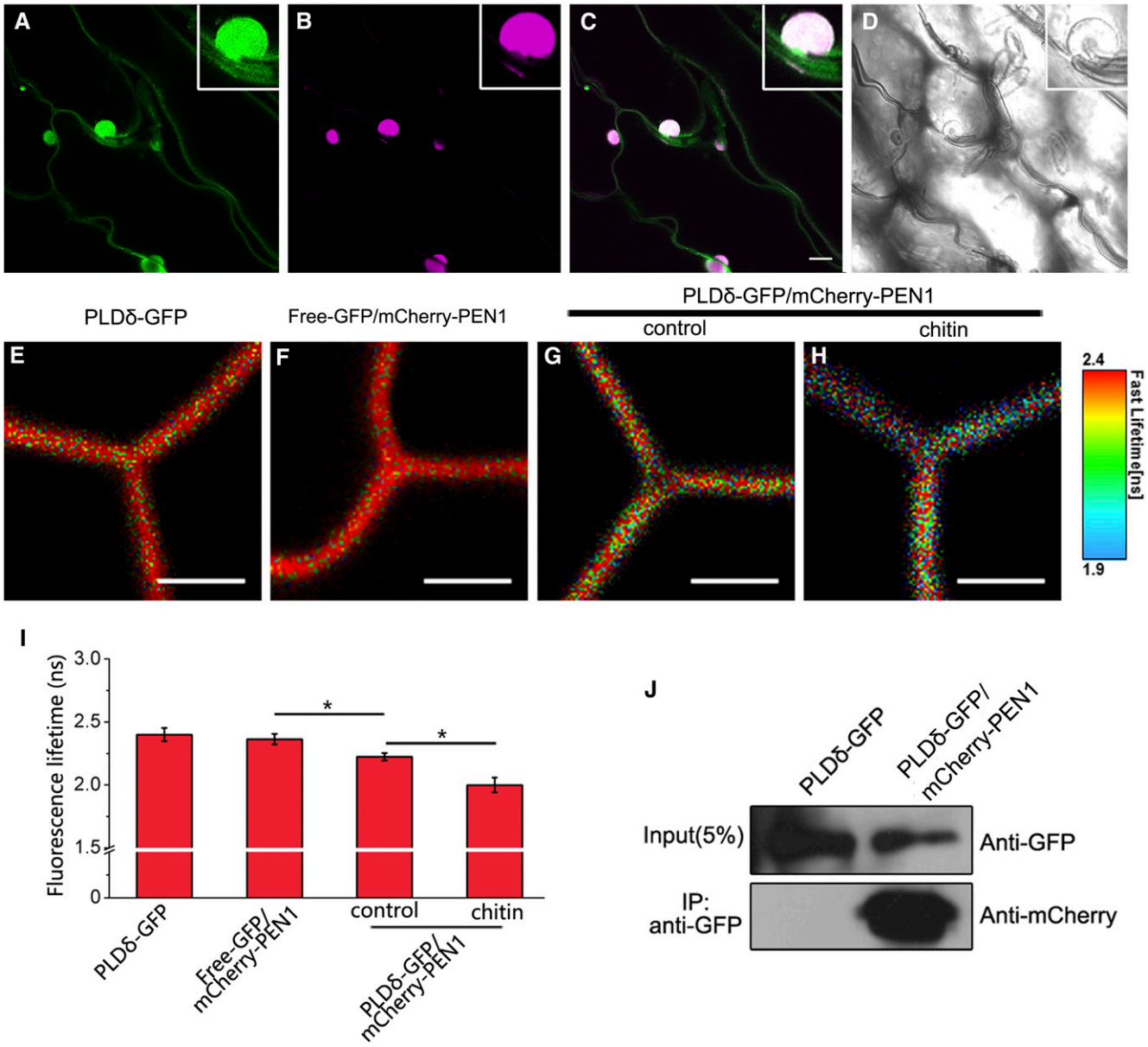

Figure 5. Colocalization and Interaction Analysis of PLDδ with PEN1 in Living Plant Cells.

(A) to **(D)** Colocalization of PLDδ-GFP **(A)** and mCherry-PEN1 **(B)** in the papillae, with the merged **(C)** and bright-field **(D)** images.

(E) to **(H)** Live-cell imaging (using confocal microscopy) of fluorescence lifetime distribution of PLDδ-GFP in the plants expressing PLDδ-GFP alone **(E)**, coexpressing free-GFP/mCherry-PEN1 **(F)**, and coexpressing PLDδ-GFP/mCherry-PEN1 (see **[G]** and **[H]**). **(G)** and **(H)** indicate the fluorescence lifetime of PLDδ-GFP with **(H)** or without chitin treatment **(G)**.

(I) FRET-FLIM analysis revealed the change in the fluorescence lifetime of PLDδ-GFP ($n = 10$, with 15 regions of interest in the plants expressing PLDδ-GFP alone and in the plants coexpressing PLDδ-GFP/mCherry-PEN1 under both control condition and chitin treatment).

(J) Coimmunoprecipitation of PEN1 with PLDδ in transgenic Arabidopsis. Total protein extracts from PLDδ-GFP and PLDδ-GFP/mCherry-PEN1 transgenic plants were immunoprecipitated with anti-GFP. Immunoprecipitated proteins were detected by immunoblotting with anti-mCherry antibody. Bars represent means; error bars in **(I)** represent SD. ANOVA and post hoc Tukey's test for **(I)**. *$P < 0.05$. Bar = 10 μm in **(A)** to **(D)**; bar = 2 μm in **(E)** to **(H)**. IP, immunoprecipitated.

Stanislas et al., 2009; Keinath et al., 2010). AtREM1.3 resides in sterol-rich microdomains in the PM (Demir et al., 2013) and is associated with fungal infection (Bozkurt et al., 2014). Our results showed that the interaction between PLDδ and AtREM1.3 was enhanced in the presence of chitin, suggesting that the pathogen-triggered, newly translated PLDδ proteins are sorted into AtREM1.3-labeled, sterol-rich microdomains. Parallel experiments using MβCD plus chitin treatment showed that sterol depletion led to decreased PLDδ-GFP accumulation and lower PA production. Since distinct subcellular localizations of PLDs led to

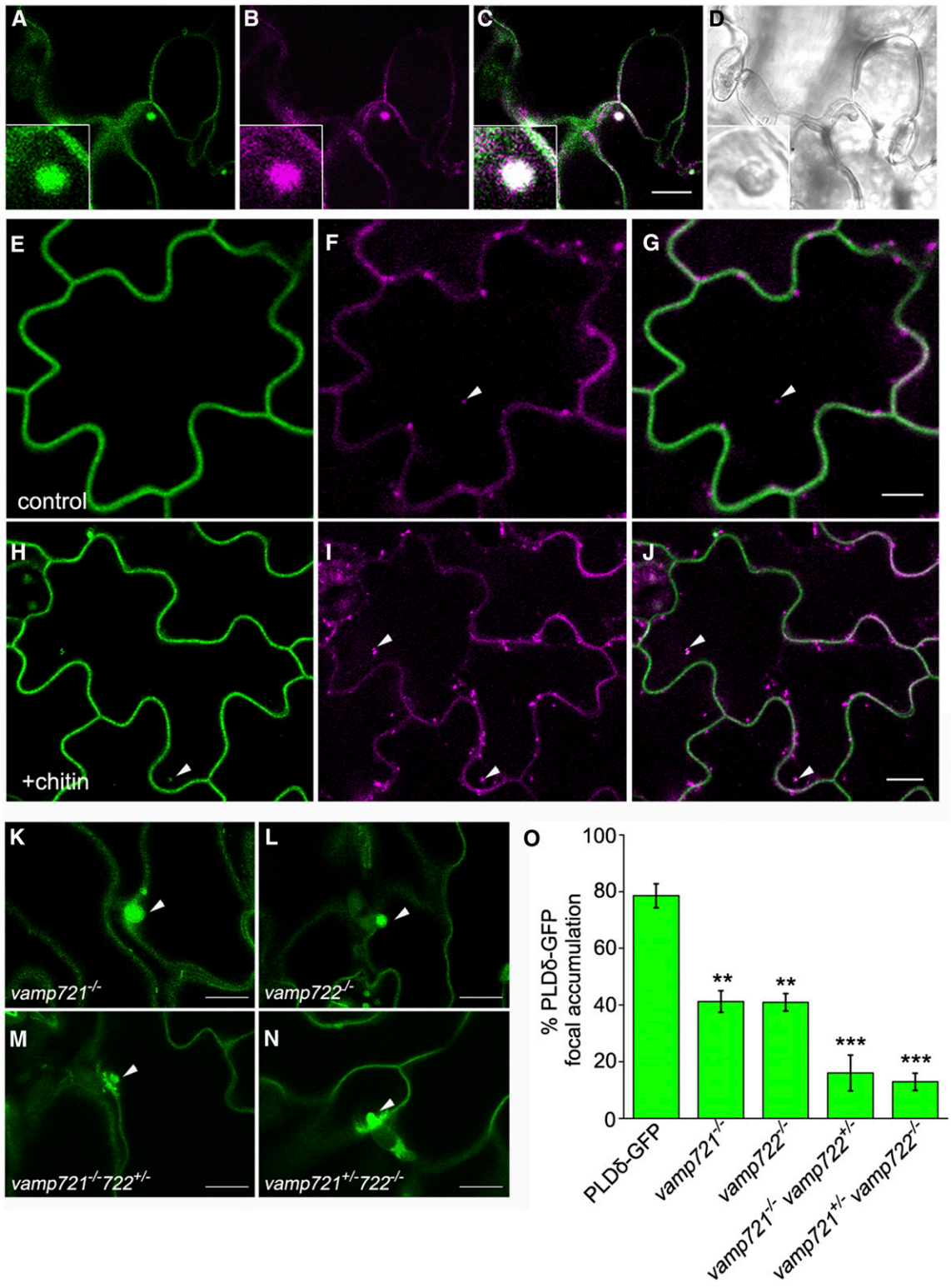

Figure 6. PLDδ Is Trafficked to the Papillae via VAMP721/722-Mediated Secretion in Response to Chitin.

(A) to **(D)** Colocalization of PLDδ-GFP **(A)** and mCherry-VAMP721 **(B)** in the papillae at the *Bgh* infection sites, with the merged **(C)** and bright-field **(D)** images. **(E)** to **(J)** Colocalization (see **[G]** and **[J]**) of PLDδ-GFP (see **[E]** and **[H]**) and mCherry-VAMP721 (see **[F]** and **[I]**) in the cytoplasm under control conditions (see **[E]** to **[G]**) or chitin treatment (see **[H]** to **[J]**). Arrowheads indicate the cytoplasmic bodies labeled by GFP or mCherry.

the production of PA at specific regions of cell membranes (Liu et al., 2013), and PLDs might be recruited to subdomains at the PM (Novák et al., 2018), we proposed that the microdomain localization of PLDδ contributes to the activation of PLDδ and might be related to the local production of the lipid secondary messenger PA.

In exocytosis, membrane-bound vesicles fuse with the PM and release their contents to the outside, a process that is closely involved with plant immunity (Kwon et al., 2008a). Accumulating evidence from studying the interaction of Arabidopsis with the *Bgh* fungus points to a key role of exocytosis in plant innate immunity (Yun and Kwon, 2017). Although substantial genetic analysis has focused on the pathogen-trigged immune response, the regulatory mechanism of exocytosis in plant–pathogen interactions has largely been neglected. In the present study, we detected a rapid recovery and an increased exocytosis rate of PLDδ after stimulation by chitin. From the different recovery rates after photobleaching, we conclude that the PLDδ was rapidly recruited from the cytoplasm to the PM by secretion following chitin treatment and that exocytosis provides a fast and efficient way to control PLDδ activity in response to pathogen attack.

In plants, exocytosis via the endomembrane system and secreted proteins are crucial for cell wall deposition and modification in response to biotic stimuli (Surpin and Raikhel, 2004). The ADP ribosylation factor/guanine nucleotide exchange factor inhibitor BFA, a well-known inhibitor of secretory and endocytic pathways, is a useful diagnostic tool for recognizing the mode of exocytosis (Kleine-Vehn et al., 2006; Beck et al., 2012; Ding et al., 2014). In our study, no conventional signal peptide sequence was found in PLDδ predicted by the SignalP 5.0 server (http://www.cbs.dtu.dk/services/SignalP/) or the TargetP 2.0 server (http://www.cbs.dtu.dk/services/TargetP/), indicating that PLDδ was exported by a signal peptide-independent secretory process. We further found that the secretion of PLDδ can occur in both BFA-resistant and BFA-sensitive manners. The BFA-resistant pathway of PLDδ appears to be unaffected in response to pathogen stimuli, while the exocytosis of PLDδ by the BFA-sensitive pathway significantly increased. These findings suggested that PLDδ may constitutively be recycled in a BFA-resistant manner in resting conditions, but upon perception of pathogen, the BFA-sensitive pathway is dramatically enhanced. These observations provide strong evidence that plants have evolved a mechanism to respond to pathogen attack by a trade-off that alters the dynamic equilibrium between BFA-resistant and -sensitive exocytic pathways.

Vesicle trafficking functions as a vital part of the extracellular immune response to ascomycete pathogens in Arabidopsis (Collins et al., 2003; Kwon et al., 2008b). Vesicle-associated secretion mediated by PEN1 and its SNARE partners SNAP33 and endomembrane-resident VAMP721/722 can enable the execution of penetration resistance, and this secretion pathway can be blocked by treatment with BFA (Nielsen et al., 2012; Underwood and Somerville, 2013; Zhang et al., 2019). In our study, BFA effectively blocked the secretion and accumulation of PLDδ-GFP, which was similar to its effect on PEN1. Moreover, we found that chitin significantly enhanced the colocalization and interaction of PLDδ-GFP and mCherry-PEN1, and the deficiency of VAMP721/722 led to a decrease in papillary PLDδ-GFP accumulation. Taken together, these findings demonstrated that PEN1-associated, VAMP721/722-mediated secretion enables the translocation of PLDδ during attack by powdery mildew fungi.

PA generated by PLDs is considered as a secondary messenger and interacts with effector proteins such as protein kinases, phosphatases, and NADPH oxidases, modulating their activity and thus amplifying the signal to initiate plant defense signaling (Rizzo et al., 2000; Rentel et al., 2004; Wang et al., 2006). Zhang et al. (2018) reported that *PLDδ* knockout plants showed enhanced susceptibility to lettuce powdery mildew (*Golovinomyces cichoracearum*, *Gc* UCSC1), but they did not detect the changes of JA levels after 5 d postinfection under *Gc* UCSC1 attack (Zhang et al., 2018). In our study, we observed that *pldδ* mutants exhibited markedly lower levels of PA, H_2O_2, and JA than the wild-type plants, partly due to the differences in the timing of examination and different effects on JA levels induced in various pathogen species. Likewise, the genes related to PA, reactive oxygen species, and JA signaling were downregulated in *pldδ* mutants compared with the wild-type plants, indicating that the absence of PLDδ disturbed the plants' ability to produce H_2O_2 and JA in response to the chitin stimulus. Moreover, *snare* mutants and *pldδ* mutants showed similar phenotypes in response to pathogen stimuli, suggesting that the delivery of PLDδ mediated by the SNARE complex contributed to the resistance function of PLDδ. In combination with the accumulation of PA at papillae, these findings support the hypothesis that the translocation of PLDδ to papillae depends on a PEN1/VAMP721/722-mediated secretion pathway, which is accompanied by PLDδ activation and production of PA, thus triggering PA-mediated signaling in the plant defense response.

In summary, our investigation of the dynamic behaviors of PLDδ has provided a more global view of the mechanism of translocation of this phospholipase in the immune response to pathogens. The focal concentration of PLDδ at pathogen entry sites is important for its function and is regulated by diverse secretory pathways. Consequently, PM microdomains likely harbor unique sets of signaling proteins or serve as signaling platforms in penetration resistance, acting as transfer stations to deliver

Figure 6. (continued).

(K) to **(N)** Fluorescence images demonstrating the accumulation of PLDδ-GFP at the penetration sites of *Bgh* in PLDδ-GFP *vamp721*$^{-/-}$ **(K)**, PLDδ-GFP *vamp722*$^{-/-}$ **(L)**, PLDδ-GFP *vamp721*$^{+/-}$ *vamp722*$^{-/-}$ **(M)**, and PLDδ-GFP *vamp721*$^{-/-}$ *vamp722*$^{+/-}$ **(N)** plants. The white arrowheads in **(K)** to **(N)** indicate the accumulation of PLDδ-GFP.

(O) Number of foci was enumerated for at least 49 germinated spores per leaf for six leaves per genotype ($n = 6$). Bars represent means; error bars in all panels represent SD. ANOVA and post hoc Tukey's test, $^{**}P < 0.01$, $^{***}P < 0.001$. Bar in **(A)** to **(N)** = 10 μm.

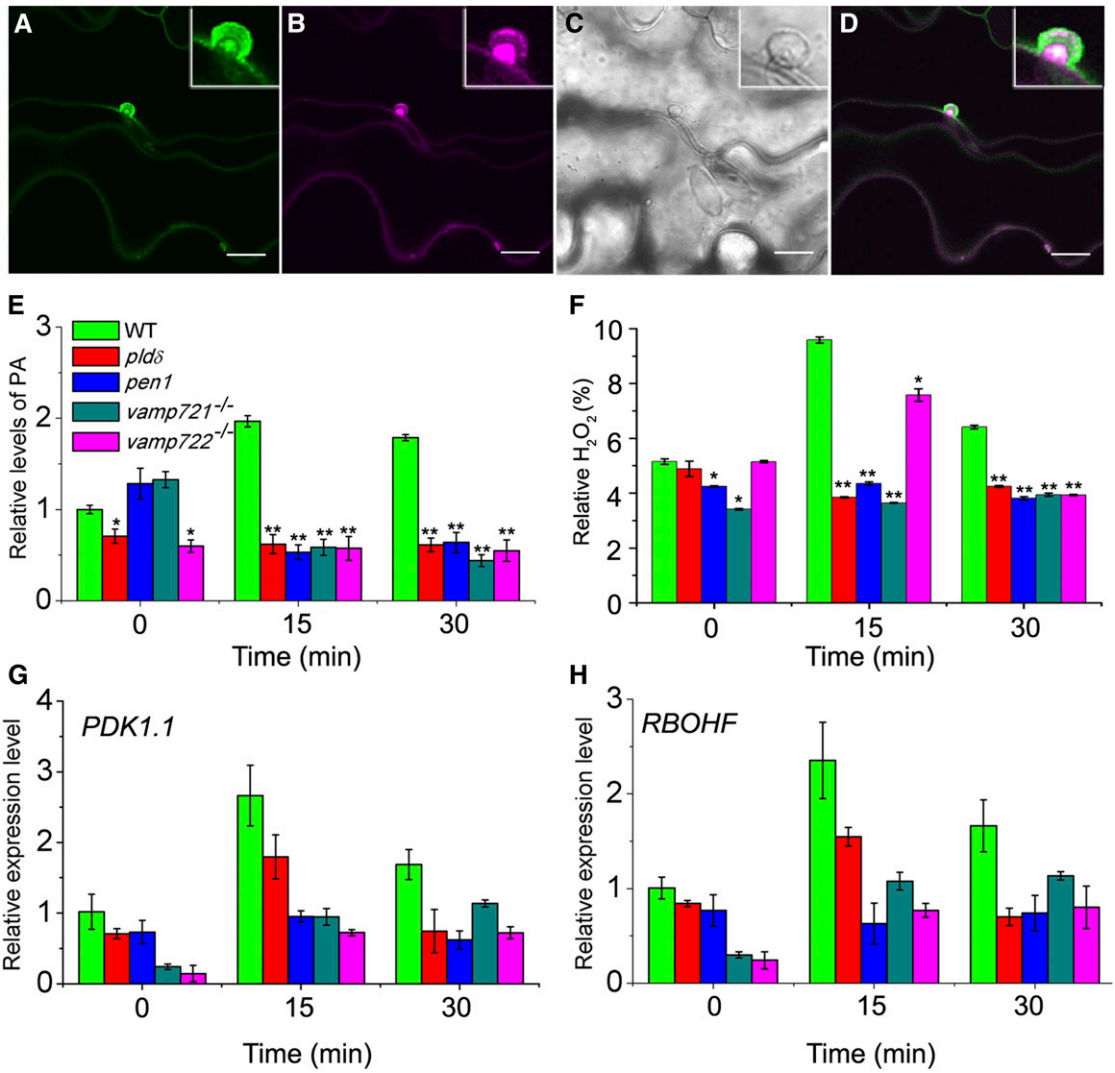

Figure 7. PA Levels, Reactive Oxygen Accumulation, and Defense-Related Gene Expression in the Absence of PLDδ and the SNARE Complex in Response to Pathogen Stimuli.

(A) to **(D)** Focal accumulation of PLDδ-GFP **(A)** and a fluorescent PA biosensor **(B)** in the papillae at the *Bgh* entry site, with bright-field **(C)** and merged **(D)** images. The PA sensor is the PA binding domain of the yeast SNARE Spo20p fused to the fluorescent protein mCherry.

(E) Total PA in Col-0, *pldδ*, *pen1*, *vamp721*$^{-/-}$, and *vamp722*$^{-/-}$ plants measured by mass spectrometry under chitin treatment for 0, 15, and 30 min. Relative PA levels compared to the wild type at time 0 (control) are presented. WT, wild type.

(F) Total H_2O_2 in Col-0, *pldδ*, *pen1*, *vamp721*$^{-/-}$, and *vamp722*$^{-/-}$ plants measured by a micro H_2O_2 assay kit under chitin treatment for 0, 15, and 30 min. Relative H_2O_2 levels compared to the wild type at time 0 (control) are presented.

(G) and **(H)** Expression of defense-related genes in *Col-0*, *pldδ*, *pen1*, *vamp721*$^{-/-}$, and *vamp722*$^{-/-}$ mutant plants in response to chitin. Transcript levels were normalized to *ACTIN2*. Relative expression levels compared to the wild type at time 0 (control) are presented. Data bars represent the mean ± SD of three repeats. The asterisk (*) in **(E)** and **(F)** indicates the statistically significant difference in the level of PC and phosphatidylethanolamine compared to respective control. Student's *t* test, *P < 0.05, **P < 0.01. Bar = 10 μm in **(A)** to **(D)**.

pathogen-inducible PLDδ to the papillae. This study produced three novel findings: (1) secretion of PLDδ functions as a fast and efficient way to control PLDδ accumulation in response to pathogen attack; (2) plants have evolved a dynamic equilibrium between BFA-resistant and -sensitive exocytic pathways in the secretion of PLDδ under diverse conditions, and the exocytosis of pathogen-inducible PLDδ in BFA-sensitive manner requires PEN1-associated VAMP721/722-mediated secretion; and (3) AtREM1.3-labeled, sterol-rich microdomains act as essential platforms for the transportation and accumulation of PLDδ. Taken together, these findings reveal a novel regulatory mechanism involving membrane microdomains and exocytosis in the relocalization of PLDδ, aiding in the execution of penetration resistance against a fungal pathogen.

METHODS

Plant and Fungal Growth

The Arabidopsis (*Arabidopsis thaliana*) *pldδ* mutant expressing the transgene *PLDδ-GFP* driven by the endogenous *PLDδ* promoter and the *pldδ* mutant (SALK_023247) was used in all experiments (Pinosa et al., 2013). The *p35S:AtREM1.3-mCherry* vectors were described previously (Xue et al., 2018). The *vamp721*$^{-/-}$, *vamp722*$^{-/-}$, *vamp721*$^{+/-}$ *vamp722*$^{-/-}$, and *vamp721*$^{-/-}$ *vamp722*$^{+/-}$ mutants and Arabidopsis expressing the transgene *pVAMP721/722:mCherry-VAMP721/722* were obtained from Zhang et al. (2011). The *p35S:AtREM1.3-mCherry* vectors were transformed into Col-0, and seedlings were selected with 70 μg/mL hygromycin. For Arabidopsis coexpressing PLDδ-GFP and mCherry-PEN1, PLDδ-GFP and mCherry-VAMP721/722, and PLDδ-GFP and AtREM1.3-mCherry, F1 lines derived from crosses between PLDδ-GFP and mCherry-PEN1, mCherry-VAMP721/722, or AtREM1.3-mCherry, respectively. The plants were grown at 21°C, with 12 h of white light (light intensity of 120 μmol photons m^{-2} s^{-1}) per day. The barley powdery mildew fungus (*Blumeria graminis* f. sp *hordei*, isolate K1) was propagated on barley (*Hordeum vulgare*) at 18°C in an illuminated incubator.

Drug Treatments

The inhibitors BFA, CHX, and MβCD were obtained from Sigma-Aldrich. CHX and BFA were made into stock solutions with DMSO (50 mM for CHX and 50 mM for BFA), and MβCD was dissolved in deionized water to yield a 200 mM stock solution. The PAMP chitin solutions were generated by dissolving hydrolyzed chitin (purified from crab shells; Sigma-Aldrich) in deionized water to a concentration of 100 μg·mL^{-1}. FM4-64 (Invitrogen) was kept as a 5 mM stock solution and diluted to a 5 μM working solution with half-strength liquid Murashige and Skoog (MS) medium. The BFA treatment combined with fungal inoculation was performed as described previously by Nielsen et al., (2012). For other inhibitor treatments, seedlings were incubated in half-strength liquid MS medium containing appropriate drugs for the following times: 30 min for BFA, 30 min of pretreatment with BFA and 30 min for BFA plus 100 μg·mL^{-1} chitin, 30 min for MβCD, and 30 min pretreatment with MβCD plus 100 μg·mL^{-1} chitin. Seedlings were then transferred onto a slide with inhibitor solution and covered with a cover slip for confocal laser scanning microscopy or variable angle (VA)–TIRFM imaging.

FM4-64 Detection, Plasmolysis, and FRAP Analysis Using Confocal Microscopy

The leaves from adult Arabidopsis plants were dipped in a solution of 0.01% (v/v) Silwet, 0.2% (w/v) propidium iodide to stain the *Blumeria graminis* f. sp *hordei* (*Bgh*) spores (Nielsen et al., 2012). Membrane staining was performed by incubating the adult leaves with 3 μM FM4-64 for 30 min before observation, and plasmolysis experiments were conducted by incubating the adult leaves with 1 M mannitol for 5 min before observation. An FV1000ME multiphoton laser scanning microscope (Olympus) was used to observe the FRAP of the plants, and 488- and 458-nm laser lines operating at 100% were used to bleach the PLDδ-GFP from a region of the same size in every treatment. Images were collected 1 min before bleaching, immediately after bleaching, and once a minute after bleaching for a total of 20 min. The fluorescence recovery data obtained were corrected for bleaching during imaging as described previously by Konopka et al., (2008) and Underwood and Somerville, (2013), and fitted curves were made using Origin 8.0 software (OriginLab). The exocytosis rate was calculated according to the methods described previously by Luo et al., (2016).

VA-TIRFM and Single-Particle Fluorescence Image Analysis

The PLDδ-GFP dynamics was recorded using a VA-TIRFM technique on an inverted microscope (IX-71, Olympus) with a total internal reflective fluorescence illuminator and a 100× oil immersion objective (Olympus; numerical aperture = 1.45; Li et al., 2011, 2012; ; Fan et al., 2013; Wang et al., 2013, 2015a, 2015b, 2018). The method described by Wang et al. (2015b) was used for single-particle tracking, which was the basis of the kinetic parameter analysis of PLDδ-GFP. The diffusion coefficient (*D*) was determined according to the methods described previously by Xiao et al., (2008), Li et al., (2011), and Wang et al., (2015b). Trajectories with a length of >10 frames were kept for MSD and diffusion coefficient analysis. The MSD calculation of PLDδ-GFP spots was performed using the following equation:

$$\mathrm{MSD}(t)=\frac{1}{L-n}\sum_{s=0}^{L-n-1}(\boldsymbol{r}(s+n)-\boldsymbol{r}(s))^2 \quad (1)$$

where $n = t/\Delta t$, L is the length of the trajectory, and $\boldsymbol{r}(s)$ is the two-dimensional position of the particle in frames (Goulian and Simon, 2000). The D for a spot was determined by fitting a line to MSD with n running from 1 to the largest integer $\leq L/4$ (Saxton, 1997). In the text, a single (or multiple) Gaussian t(s) of the D histograms represents the diffusion coefficients of PLDδ-GFP spots. Origin software (OriginLab) was used to determine the SE values of the position of the peak (denoted $\hat{G}$) in the form of an upper and a lower D. Moreover, parameters were performed according to Espenel et al., (2008) and used to determine the motional modes (Brownian, restricted diffusion). When linearly fitted to the MSD, the MSD-t plot was a straight line with a slope of 4D, representing a typical trajectory for spots undergoing Brownian diffusion. If the MSD-t plot showed a negative deviation from a straight line with a slope of 4D, the motion was defined as restricted diffusion. Single fluorescent spots of PLDδ-GFP were detected in a time-lapse series of up to 100 images per sequence, which were acquired with a 200-ms exposure time.

FCS and PPI Analysis

The FCS analysis was performed using the point-scanning mode on a TCS SP5 FCS microscope (Leica) equipped with a 488-nm argon laser, in-house coupled correlator, and Avalanche photodiode. Spontaneous fluctuations in fluorescence intensity were generated by the diffusion of PLDδ-GFP molecules in and out of the focal plane, which can alter the local concentration of the fluorophores. The density of PLDδ-GFP was detected by a laser focused at the PM and calculated according to the protocol previously described by Li et al. (2011). PPI was performed on confocal images using PPI software (Wu et al. 2010; Zinchuk et al. 2013; Cui et al., 2019). The quantification of the degree of colocalization between PLDδ-GFP and mCherry-PEN1 or AtREM1.3-mCherry was based on the review by Zinchuk et al. (2013).

FRET-FLIM Analysis

FRET-FLIM analysis was performed using an inverted FV1200 microscope (Olympus) equipped with a PicoQuant picoHarp300 controller. The excitation at 488 nm was performed by a picosecond pulsed diode laser at a repetition rate of 40 MHz, via a water immersion objective (60×, numerical aperture = 1.2). The emitted light was filtered with a 520/35-nm bandpass filter and detected by an MPD SPAD detector. Data were collected and analyzed using the SymphoTime 64 software (PicoQuant).

Coimmunoprecipitation and Immunoblot Analysis

To monitor the abundance of PLDδ-GFP in the different treatment groups, total proteins were extracted from the PLDδ-GFP transgenic plants grown

on half-strength MS medium for 3 weeks using the EZ extraction protocol (Martínez-García et al., 1999). For membrane protein extraction, the PLDδ-GFP plants were ground into a fine powder in liquid nitrogen and mixed with extraction solution (25 mM Tris, pH 7.5, 2 mM EDTA, 2 mM DTT, 15 mM mercaptoethanol, 0.5% [w/v] BSA, 0.25 M Suc, 10% [v/v] glycerol, and 1 complete protease inhibitor tablet [Roche Applied Science] per 50 mL of extraction buffer). After being mixed in a 1:1 (v/v) ratio with SDS-PAGE buffer, the protein extraction solution was heated at 95°C for 15 min and then centrifuged at 12,000 rpm (10,625*g*) for 5 min to remove cellular debris. The supernatants containing total proteins and membrane proteins were subjected to 8% SDS-PAGE. An immunoblot analysis was performed following the protocol described by Fan et al. (2013). For coimmunoprecipitation, plants coexpressing PLDδ-GFP and mCherry-PEN1 were harvested, and the assay was performed as described previously by Serino and Deng, (2007) and Fan et al., (2013).

PA Analysis by Mass Spectrometry and PLD Activity Assay

For PA extraction, the seedlings of every genotype were harvested under chitin treatment for 0, 15, and 30 min. The harvested seedlings were transferred immediately into 2 mL of isopropanol with 0.01% (v/v) butylated hydroxytoluene at 75°C. Chloroform/methanol (2:1) was used to extract the tissue three additional times with 2 h of agitation each time. Next, the tissues were heated overnight at 105°C and weighed. A triple quadrupole tandem mass spectrometer equipped for electrospray ionization was used to analyze lipid samples. The PAs in each class were quantified by comparison with two internal standards for the class. Data processing was performed as described previously (Welti et al., 2002).

PLD activity was assayed spectrophotometrically by measuring the free choline released upon PC hydrolysis. Plant tissues were harvested under resting condition and the treatments of chitin, MβCD, and MβCD plus chitin. The harvested tissues were then incubated with PC substrate, and the reaction mixture containing 50 mM Tris-HCl, pH 8.0, 20 mM $CaCl_2$, 1.7 mM 4-aminoantipyrine, 9 mM sodium 2-hydroxy-3, 5-dichlorobenzenesulfonate, 0.5 unit of choline oxidase, and 0.5 unit of peroxidase for 30 min at 30°C. The absorbance measurements at 500 nm were performed to quantify the amounts of free choline released. One unit of PLD activity was calculated as described in a previous study (Abdelkafi and Abousalham, 2011).

Statistics

All experimental analyses were conducted in consultation with a statistician. Quantification and statistical parameters are reported in legends of each figure, including error bars (SD or SE), *n* values, repeats of experiments, and test types. Student's *t* test was used to describe differences between two groups. For those involving multiple group comparisons, ANOVA followed by a post hoc test was applied. In the figures, statistically significant differences are shown with asterisks as follows: *P < 0.05, **P < 0.01, and ***P < 0.001.

Accession Numbers

Sequence data from this article can be found in The Arabidopsis Information Resource database under the following accession numbers: *PLD*δ (AT4G35790), *AtRem1.3* (At2g45820), *VAMP721* (AT1G04750), *VAMP722* (AT2G33120), and *PEN1* (AT3G11820).

Supplemental Data

Supplemental Figure 1. PLDδ is involved in non-host resistance to *Bgh* (supports Figure 1).

Supplemental Figure 2. The abundance of PLDδ-GFP is influenced by CHX (supports Figure 2).

Supplemental Figure 3. FRAP analysis revealing the dynamics of PLDδ-GFP with or without stimulation by chitin (supports Figure 2).

Supplemental Figure 4. Dynamics of PLDδ-GFP at the plasma membrane estimated by FRAP (supports Figure 2).

Supplemental Figure 5. The effect of MβCD on PLDδ-GFP dynamics (supports Figure 3).

Supplemental Figure 6. The levels of phosphatidic acid and PLD activity under stimulation of pathogen (supports Figure 3).

Supplemental Figure 7. MβCD blocked the accumulation of PLDδ-GFP at the *Bgh* entry sites (supports Figure 3).

Supplemental Figure 8. Penetration rate of *Bgh* affected by MβCD or BFA (supports Figure 3 and Figure 4).

Supplemental Figure 9. Subcellular localization of PLDδ in the presence of CHX (Supports Figure 4).

Supplemental Figure 10. The colocalization of PLDδ-GFP and mCherry-PEN1 analyzed by protein proximity index (supports Figure 5).

Supplemental Figure 11. The colocalization of PLDδ-GFP and mCherry-VAMP722 in the cytoplasm and papillae (supports Figure 6).

Supplemental Figure 12. Relative levels of PC and PE levels in the absence of PLDδ and the SNARE complex in response to pathogen stimuli (supports Figure 7).

Supplemental Figure 13. JA level and expression of JA-related genes in wild-type, *pld*δ, *pen1*, *vamp721*$^{-/-}$, and *vamp722*$^{-/-}$ mutant plants in response to chitin (supports Figure 7).

Supplemental Table. Primers used for qPCR.

Supplemental Movie 1. VA-TIRFM imaging of PLDδ-GFP spots in the control condition at the PM of Arabidopsis leaf epidermal cells.

Supplemental Movie 2. VA-TIRFM imaging of PLDδ-GFP spots at the PM of Arabidopsis leaf epidermal cells under chitin treatment.

Supplemental Movie 3. VA-TIRFM imaging of PLDδ-GFP spots at the PM of Arabidopsis leaf epidermal cells treated with 10 mM MβCD.

Supplemental Movie 4. VA-TIRFM imaging of PLDδ-GFP spots at the PM of Arabidopsis leaf epidermal cells under MβCD + chitin treatment.

AUTHOR CONTRIBUTIONS

J.J.X., X.J.L., X.H.W., and J.X.L. designed the research; J.J.X. and X.Q.L. performed the research; J.J.X., X.J.L., L.W., X.Q.L., and L.Z. analyzed data; J.J.X., X.J.L., Q.H.S., F.B., M.B., J.S., Y.F.Z., and J.X.L. wrote the article.

We thank Mats X. Andersson (University of Gothenburg, Sweden) for kindly providing the transgenic seeds expressing *PLD*δ*-GFP* driven by the endogenous *PLD*δ promoter and the *pld*δ mutant. We also thank Ying Fu (China Agricultural University, Beijing) for kindly providing the seeds expressing the transgene *pPEN1*::*mCherry-PEN1*. We thank the members of the Imaging Core Facility, Technology Center for Protein Sciences (Tsinghua University), for assistance with using the FV1200 LSCM with the Picoquant FLIM/FCS system. This work is supported by the National Natural Science Foundation of China (grants 31530084, 31622005, and 31900162), the Program of Introducing Talents of Discipline to Universities

(111 project, B13007), and the European Regional Development Fund (ERDF) project "Plants as a tool for sustainable global development" (grant CZ.02.1.01/0.0/0.0/16_019/0000827).

Received July 15, 2019; revised September 20, 2019; accepted October 6, 2019; published October 9, 2019.

REFERENCES

Abdelkafi, S., and Abousalham, A. (2011). The substrate specificities of sunflower and soybean phospholipases D using trans-phosphatidylation reaction. Lipids Health Dis. **10:** 196.

An, Q., Hückelhoven, R., Kogel, K.H., and van Bel, A.J. (2006). Multivesicular bodies participate in a cell wall-associated defence response in barley leaves attacked by the pathogenic powdery mildew fungus. Cell. Microbiol. **8:** 1009–1019.

Assaad, F.F., Qiu, J.L., Youngs, H., Ehrhardt, D., Zimmerli, L., Kalde, M., Wanner, G., Peck, S.C., Edwards, H., Ramonell, K., Somerville, C.R., and Thordal-Christensen, H. (2004). The PEN1 syntaxin defines a novel cellular compartment upon fungal attack and is required for the timely assembly of papillae. Mol. Biol. Cell **15:** 5118–5129.

Bargmann, B.O., and Munnik, T. (2006). The role of phospholipase D in plant stress responses. Curr. Opin. Plant Biol. **9:** 515–522.

Beck, M., Zhou, J., Faulkner, C., MacLean, D., and Robatzek, S. (2012). Spatio-temporal cellular dynamics of the *Arabidopsis* flagellin receptor reveal activation status-dependent endosomal sorting. Plant Cell **24:** 4205–4219.

Bhat, R.A., Miklis, M., Schmelzer, E., Schulze-Lefert, P., and Panstruga, R. (2005). Recruitment and interaction dynamics of plant penetration resistance components in a plasma membrane microdomain. Proc. Natl. Acad. Sci. USA **102:** 3135–3140.

Bozkurt, T.O., Richardson, A., Dagdas, Y.F., Mongrand, S., Kamoun, S., and Raffaele, S. (2014). The plant membrane-associated REMORIN1.3 accumulates in discrete perihaustorial domains and enhances susceptibility to *Phytophthora infestans*. Plant Physiol. **165:** 1005–1018.

Clay, N.K., Adio, A.M., Denoux, C., Jander, G., and Ausubel, F.M. (2009). Glucosinolate metabolites required for an *Arabidopsis* innate immune response. Science **323:** 95–101.

Collins, N.C., Thordal-Christensen, H., Lipka, V., Bau, S., Kombrink, E., Qiu, J.L., Hückelhoven, R., Stein, M., Freialdenhoven, A., Somerville, S.C., and Schulze-Lefert, P. (2003). SNARE-protein-mediated disease resistance at the plant cell wall. Nature **425:** 973–977.

Cui, Y., Yu, M., Yao, X., Xing, J., Lin, J., and Li, X. (2018). Single-particle tracking for the quantification of membrane protein dynamics in living plant cells. Mol. Plant **11:** 1315–1327.

Cui, Y., Zhang, X., Yu, M., Zhu, Y., Xing, J., and Lin, J. (2019). Techniques for detecting protein-protein interactions in living cells: Principles, limitations, and recent progress. Sci. China Life Sci. **62:** 619–632.

Demir, F., Horntrich, C., Blachutzik, J.O., Scherzer, S., Reinders, Y., Kierszniowska, S., Schulze, W.X., Harms, G.S., Hedrich, R., Geiger, D., and Kreuzer, I. (2013). *Arabidopsis* nanodomain-delimited ABA signaling pathway regulates the anion channel SLAH3. Proc. Natl. Acad. Sci. USA **110:** 8296–8301.

Ding, Y., Robinson, D.G., and Jiang, L. (2014). Unconventional protein secretion (UPS) pathways in plants. Curr. Opin. Cell Biol. **29:** 107–115.

Espenel, C., Margeat, E., Dosset, P., Arduise, C., Le Grimellec, C., Royer, C.A., Boucheix, C., Rubinstein, E., and Milhiet, P.E. (2008). Single-molecule analysis of CD9 dynamics and partitioning reveals multiple modes of interaction in the tetraspanin web. J Cell Biol **182:** 765–776.

Fan, L., Hao, H., Xue, Y., Zhang, L., Song, K., Ding, Z., Botella, M.A., Wang, H., and Lin, J. (2013). Dynamic analysis of Arabidopsis AP2 σ subunit reveals a key role in clathrin-mediated endocytosis and plant development. Development **140:** 3826–3837.

Fujiwara, M., Hamada, S., Hiratsuka, M., Fukao, Y., Kawasaki, T., and Shimamoto, K. (2009). Proteome analysis of detergent-resistant membranes (DRMs) associated with OsRac1-mediated innate immunity in rice. Plant Cell Physiol. **50:** 1191–1200.

Gardiner, J.C., Harper, J.D., Weerakoon, N.D., Collings, D.A., Ritchie, S., Gilroy, S., Cyr, R.J., and Marc, J. (2001). A 90-kD phospholipase D from tobacco binds to microtubules and the plasma membrane. Plant Cell **13:** 2143–2158.

Goulian, M., and Simon, S.M. (2000). Tracking single proteins within cells. Biophys J **79:** 2188–2198.

Guo, L., Devaiah, S.P., Narasimhan, R., Pan, X., Zhang, Y., Zhang, W., and Wang, X. (2012). Cytosolic glyceraldehyde-3-phosphate dehydrogenases interact with phospholipase Dδ to transduce hydrogen peroxide signals in the Arabidopsis response to stress. Plant Cell **24:** 2200–2212.

Hong, Y., Zhao, J., Guo, L., Kim, S.C., Deng, X., Wang, G., Zhang, G., Li, M., and Wang, X. (2016). Plant phospholipases D and C and their diverse functions in stress responses. Prog. Lipid Res. **62:** 55–74.

Jarsch, I.K., Konrad, S.S.A., Stratil, T.F., Urbanus, S.L., Szymanski, W., Braun, P., Braun, K.H., and Ott, T. (2014). Plasma membranes are subcompartmentalized into a plethora of coexisting and diverse microdomains in *Arabidopsis* and *Nicotiana benthamiana*. Plant Cell **26:** 1698–1711.

Jia, Y., Tao, F., and Li, W. (2013). Lipid profiling demonstrates that suppressing Arabidopsis phospholipase Dδ retards ABA-promoted leaf senescence by attenuating lipid degradation. PLoS One **8:** e65687.

Kachroo, A., and Kachroo, P. (2009). Fatty acid-derived signals in plant defense. Annu. Rev. Phytopathol. **47:** 153–176.

Katagiri, T., Takahashi, S., and Shinozaki, K. (2001). Involvement of a novel *Arabidopsis* phospholipase D, AtPLDdelta, in dehydration-inducible accumulation of phosphatidic acid in stress signalling. Plant J. **26:** 595–605.

Keinath, N.F., Kierszniowska, S., Lorek, J., Bourdais, G., Kessler, S.A., Shimosato-Asano, H., Grossniklaus, U., Schulze, W.X., Robatzek, S., and Panstruga, R. (2010). PAMP (pathogen-associated molecular pattern)-induced changes in plasma membrane compartmentalization reveal novel components of plant immunity. J. Biol. Chem. **285:** 39140–39149.

Kleine-Vehn, J., Dhonukshe, P., Swarup, R., Bennett, M., and Friml, J. (2006). Subcellular trafficking of the *Arabidopsis* auxin influx carrier AUX1 uses a novel pathway distinct from PIN1. Plant Cell **18:** 3171–3181.

Konopka, C.A., Backues, S.K., and Bednarek, S.Y. (2008). Dynamics of *Arabidopsis* dynamin-related protein 1C and a clathrin light chain at the plasma membrane. Plant Cell **20:** 1363–1380.

Kwon, C., Bednarek, P., and Schulze-Lefert, P. (2008a). Secretory pathways in plant immune responses. Plant Physiol. **147:** 1575–1583.

Kwon, C., et al. (2008b) Co-option of a default secretory pathway for plant immune responses. Nature **451:** 835–840.

Laxalt, A.M., and Munnik, T. (2002). Phospholipid signalling in plant defence. Curr. Opin. Plant Biol. **5:** 332–338.

Li, R., Liu, P., Wan, Y., Chen, T., Wang, Q., Mettbach, U., Baluska, F., Samaj, J., Fang, X., Lucas, W.J., and Lin, J. (2012). A membrane microdomain-associated protein, *Arabidopsis* Flot1, is involved in a clathrin-independent endocytic pathway and is required for seedling development. Plant Cell **24:** 2105–2122.

Li, W., Li, M., Zhang, W., Welti, R., and Wang, X. (2004). The plasma membrane-bound phospholipase Ddelta enhances freezing tolerance in *Arabidopsis thaliana*. Nat. Biotechnol. **22:** 427–433.

Li, X., Wang, X., Yang, Y., Li, R., He, Q., Fang, X., Luu, D.T., Maurel, C., and Lin, J. (2011). Single-molecule analysis of PIP2;1 dynamics and partitioning reveals multiple modes of *Arabidopsis* plasma membrane aquaporin regulation. Plant Cell **23:** 3780–3797.

Lipka, U., Fuchs, R., and Lipka, V. (2008). *Arabidopsis* non-host resistance to powdery mildews. Curr. Opin. Plant Biol. **11:** 404–411.

Lipka, V., et al. (2005) Pre- and postinvasion defenses both contribute to nonhost resistance in *Arabidopsis*. Science **310:** 1180–1183.

Liu, Y., Su, Y., and Wang, X. (2013). Phosphatidic acid-mediated signaling. Adv. Exp. Med. Biol. **991:** 159–176.

Luo, N., Yan, A., and Yang, Z. (2016). Measuring exocytosis rate using corrected fluorescence recovery after photoconversion. Traffic **17:** 554–564.

Martínez-García, J.F., Monte, E., and Quail, P.H. (1999). A simple, rapid and quantitative method for preparing *Arabidopsis* protein extracts for immunoblot analysis. Plant J. **20:** 251–257.

Mishra, G., Zhang, W., Deng, F., Zhao, J., and Wang, X. (2006). A bifurcating pathway directs abscisic acid effects on stomatal closure and opening in *Arabidopsis*. Science **312:** 264–266.

Nielsen, M.E., Feechan, A., Böhlenius, H., Ueda, T., and Thordal-Christensen, H. (2012). *Arabidopsis* ARF-GTP exchange factor, GNOM, mediates transport required for innate immunity and focal accumulation of syntaxin PEN1. Proc. Natl. Acad. Sci. USA **109:** 11443–11448.

Novák, D., Vadovič, P., Ovečka, M., Šamajová, O., Komis, G., Colcombet, J., and Šamaj, J. (2018). Gene expression pattern and protein localization of Arabidopsis phospholipase D alpha 1 revealed by advanced light-sheet and super-resolution microscopy. Front. Plant Sci. **9:** 371.

Pinosa, F., Buhot, N., Kwaaitaal, M., Fahlberg, P., Thordal-Christensen, H., Ellerström, M., and Andersson, M.X. (2013). Arabidopsis phospholipase dδ is involved in basal defense and nonhost resistance to powdery mildew fungi. Plant Physiol. **163:** 896–906.

Pleskot, R., Li, J., Zárský, V., Potocký, M., and Staiger, C.J. (2013). Regulation of cytoskeletal dynamics by phospholipase D and phosphatidic acid. Trends Plant Sci. **18:** 496–504.

Rentel, M.C., Lecourieux, D., Ouaked, F., Usher, S.L., Petersen, L., Okamoto, H., Knight, H., Peck, S.C., Grierson, C.S., Hirt, H., and Knight, M.R. (2004). OXI1 kinase is necessary for oxidative burst-mediated signalling in *Arabidopsis*. Nature **427:** 858–861.

Rizzo, M.A., Shome, K., Watkins, S.C., and Romero, G. (2000). The recruitment of Raf-1 to membranes is mediated by direct interaction with phosphatidic acid and is independent of association with Ras. J. Biol. Chem. **275:** 23911–23918.

Saxton, M.J. (1997). Single-particle tracking: the distribution of diffusion coefficients. Biophy J **72:** 1744–1753.

Serino, G., and Deng, X.W. (2007). Protein coimmunoprecipitation in Arabidopsis. CSH Protoc. **2007:** pdb prot4683.

Shahollari, B., Varma, A., and Oelmüller, R. (2005). Expression of a receptor kinase in *Arabidopsis* roots is stimulated by the basidiomycete *Piriformospora indica* and the protein accumulates in Triton X-100 insoluble plasma membrane microdomains. J. Plant Physiol. **162:** 945–958.

Stanislas, T., Bouyssie, D., Rossignol, M., Vesa, S., Fromentin, J., Morel, J., Pichereaux, C., Monsarrat, B., and Simon-Plas, F. (2009). Quantitative proteomics reveals a dynamic association of proteins to detergent-resistant membranes upon elicitor signaling in tobacco. Mol. Cell. Proteomics **8:** 2186–2198.

Stein, M., Dittgen, J., Sánchez-Rodríguez, C., Hou, B.H., Molina, A., Schulze-Lefert, P., Lipka, V., and Somerville, S. (2006). *Arabidopsis* PEN3/PDR8, an ATP binding cassette transporter, contributes to nonhost resistance to inappropriate pathogens that enter by direct penetration. Plant Cell **18:** 731–746.

Surpin, M., and Raikhel, N. (2004). Traffic jams affect plant development and signal transduction. Nat Rev Mol Cell Biol **5:** 100–109.

Takáč, T., Novák, D., and Šamaj, J. (2019). Recent advances in the cellular and developmental biology of phospholipases in plants. Front. Plant Sci. **10:** 362.

Testerink, C., and Munnik, T. (2011). Molecular, cellular, and physiological responses to phosphatidic acid formation in plants. J. Exp. Bot. **62:** 2349–2361.

Underwood, W., and Somerville, S.C. (2013). Perception of conserved pathogen elicitors at the plasma membrane leads to relocalization of the *Arabidopsis* PEN3 transporter. Proc. Natl. Acad. Sci. USA **110:** 12492–12497.

Wang, C., and Wang, X. (2001). A novel phospholipase D of *Arabidopsis* that is activated by oleic acid and associated with the plasma membrane. Plant Physiol. **127:** 1102–1112.

Wang, L., Li, H., Lv, X., Chen, T., Li, R., Xue, Y., Jiang, J., Jin, B., Baluška, F., Šamaj, J., Wang, X., and Lin, J. (2015a). Spatiotemporal dynamics of the BRI1 receptor and its regulation by membrane microdomains in living *Arabidopsis* cells. Mol. Plant **8:** 1334–1349.

Wang, L., Xue, Y., Xing, J., Song, K., and Lin, J. (2018). Exploring the spatiotemporal organization of membrane proteins in living plant cells. Annu. Rev. Plant Biol. **69:** 525–551.

Wang, Q., Zhao, Y., Luo, W., Li, R., He, Q., Fang, X., Michele, R.D., Ast, C., von Wirén, N., and Lin, J. (2013). Single-particle analysis reveals shutoff control of the *Arabidopsis* ammonium transporter AMT1;3 by clustering and internalization. Proc. Natl. Acad. Sci. USA **110:** 13204–13209.

Wang, X., and Chapman, K.D. (2013). Lipid signaling in plants. Front. Plant Sci. **4:** 216.

Wang, X., Devaiah, S.P., Zhang, W., and Welti, R. (2006). Signaling functions of phosphatidic acid. Prog. Lipid Res. **45:** 250–278.

Wang, X., Li, X., Deng, X., Luu, D.T., Maurel, C., and Lin, J. (2015b). Single-molecule fluorescence imaging to quantify membrane protein dynamics and oligomerization in living plant cells. Nat. Protoc. **10:** 2054–2063.

Welti, R., Li, W., Li, M., Sang, Y., Biesiada, H., Zhou, H.E., Rajashekar, C.B., Williams, T.D., and Wang, X. (2002). Profiling membrane lipids in plant stress responses. Role of phospholipase D alpha in freezing-induced lipid changes in Arabidopsis. J. Biol. Chem. **277:** 31994–32002.

Wu, W.Q., Zhu, X., and Song, C.P. (2019). Single-molecule technique: A revolutionary approach to exploring fundamental questions in plant science. New Phytol. **223:** 508–510.

Wu, Y., Eghbali, M., Ou, J., Lu, R., Toro, L., and Stefani, E. (2010). Quantitative determination of spatial protein-protein correlations in fluorescence confocal microscopy. Biophys. J. **98:** 493–504.

Xiao, Z., Ma, X., Jiang, Y., Zhao, Z., Lai, B., Liao, J., Yue, J., and Fang, X. (2008). Single-molecule study of lateral mobility of epidermal growth factor receptor 2/HER2 on activation. J. Phys. Chem. B **112:** 4140–4145.

Xue, Y., et al. (2018) Arabidopsis blue light receptor phototropin 1 undergoes blue light-induced activation in membrane microdomains. Mol. Plant **11:** 846–859.

Young, S.A., Wang, X., and Leach, J.E. (1996). Changes in the plasma membrane distribution of rice phospholipase D during resistant interactions with *Xanthomonas oryzae pv oryzae*. Plant Cell **8:** 1079–1090.

Yun, H.S., and Kwon, C. (2017). Vesicle trafficking in plant immunity. Curr Opin Plant Biol **40:** 34–42.

Zhang, L., Xing, J., and Lin, J. (2019). At the intersection of exocytosis and endocytosis in plants. New Phytol..

Zhang, L., Zhang, H., Liu, P., Hao, H., Jin, J.B., and Lin, J. (2011). *Arabidopsis* R-SNARE proteins VAMP721 and VAMP722 are required for cell plate formation. PLoS One **6:** e26129.

Zhang, Q., Berkey, R., Blakeslee, J.J., Lin, J., Ma, X., King, H., Liddle, A., Guo, L., Munnik, T., Wang, X., and Xiao, S. (2018). Arabidopsis phospholipase Dα1 and Dδ oppositely modulate EDS1- and SA-independent basal resistance against adapted powdery mildew. J. Exp. Bot. **69:** 3675–3688.

Zhang, W., Wang, C., Qin, C., Wood, T., Olafsdottir, G., Welti, R., and Wang, X. (2003). The oleate-stimulated phospholipase D, PLDdelta, and phosphatidic acid decrease H2O2-induced cell death in *Arabidopsis*. Plant Cell **15:** 2285–2295.

Zinchuk, V., Wu, Y., and Grossenbacher-Zinchuk, O. (2013). Bridging the gap between qualitative and quantitative colocalization results in fluorescence microscopy studies. Sci. Rep. **3:** 1365.